

Exploring the Connections between Yielding and Microscopic Irreversibility in Athermal Amorphous Rafts

A Thesis

Submitted in partial fulfillment for the degree of

MASTER OF SCIENCE

as a part of Integrated Ph. D. programme

(Materials Science)

by

NEELIMA KANDULA



CHEMISTRY AND PHYSICS OF MATERIALS UNIT
JAWAHARLAL NEHRU CENTRE FOR ADVANCED SCIENTIFIC
RESEARCH

(A Deemed University)

Bangalore – 560 064

APRIL 2014

DECLARATION

I hereby declare that the matter embodied in the thesis entitled “**Exploring the Connections between Yielding and Microscopic Irreversibility in Athermal Amorphous Rafts**” is the result of investigations carried out by me at the Chemistry and Physics of Materials Unit, Jawaharlal Nehru Centre for Advanced Scientific Research, Bangalore, India under the supervision of Dr. Rajesh Ganapathy and that it has not been submitted elsewhere for the award of any degree or diploma.

In keeping with the general practice in reporting scientific observations, due acknowledgment has been made whenever the work described is based on the findings of other investigators.

Neelima Kandula

CERTIFICATE

I hereby certify that the matter embodied in this thesis entitled “**Exploring the Connections between Yielding and Microscopic Irreversibility in Athermal Amorphous Rafts**” has been carried out by Ms. Neelima Kandula at the Chemistry and Physics of Materials Unit, Jawaharlal Nehru Centre for Advanced Scientific Research, Bangalore, India under my supervision and that it has not been submitted elsewhere for the award of any degree or diploma.

Dr. Rajesh Ganapathy
(Research Supervisor)

Acknowledgments

I would like to express my sincere gratitude to my research supervisor, Dr Rajesh Ganapathy for suggesting me an interesting and innovative research problem. I am thankful to his guidance added with support and encouragement throughout my project.

I sincerely thank Prof. C. N. R. Rao, FRS for being a constant source of inspiration and for providing excellent research facilities. I greatly admire his enthusiasm towards science.

I would like to thank CPMU Chairman, Prof. S Balasubramanian and Integrated PhD Coordinator, Dr. T K Maji for providing me a great opportunity to be part of JNCASR and for their constant support and encouragement in all the three years.

I specially thank my collaborator, Hima K Nagamanasa for assisting me in every step of my project and for many useful discussions I had with her.

I wish to thank Prof. A K Sood (IISc Bangalore) for the stimulating discussions I had with him regarding the project.

I express my warm regards to Prof. S. Balasubramanian, Prof. Alok Nath Chakravarty, Prof. Chandrabhas Narayana, Prof. K. S. Narayana, Prof. G. U. Kulkarni, Prof. A. Sundresan, Prof. S. M. Shivaprasad, Dr. Sridhar Rajaram, Dr. Rajesh Ganapathy, Dr. M. Eswaramurthy, Dr. Ranjan Dutta, Dr. Subir Das,

Prof. N. S. Vidhyadhiraja, Prof. Umesh Waghmare, Prof. Shobana Narasimhan, Prof. H. Ila, Dr. A Govindaraj, Prof. Chandan Das Gupta, Dr. Jayadeep Basu for teaching me various courses in three years during my M.S. I thank all the teaching assistants Narendra Anna, Mallikarjun, Rana Saha, Manasa, Varun, Arpan, Suresh, Sandeep, Rajdeep, Chaitanya Sharma, Nisha, Kanchan, Subhajit for helping me in experiments and my course work during my M.S.

I would like to thank all my labmates, Manasa, Srishti, Chandan, Amritha, Shreyas, Vikram, Dibyasree and Pavan for their support and help all the time.

I also thank Soumik and pallabi for helping me with the compilation of this project.

I thank all my friends - Debopreeti, Pallabi, Monali, Susheela, Sashi, Dipanwita, Sonu, Raaghesh, Krishnendu, Mohini Mohan, Ankush, Abhijit, Komal, Rajib, Uttam, Suchitra, for being with me in all my happy and sad times and helping me in need.

I thank my school and college teachers Dr. E Chakrapani, Dr. G Sahaya Bhaskaran, Dr. Ramana Murthy, Narasimha Sarma for sharing their knowledge with me and encouraging me to pursue a challenging career.

I express my deep immense respect to my parents for inspiring me and encouraging me to pursue a career in science. I thank my sister for being with me in all my happy and sad times.

I express my deep gratitude and respect to all the Gurus who enlightened me towards the TRUTH.

Preface

This thesis consists of three chapters. First chapter gives an introduction to structural glasses and sheared glasses. We have also motivated our work with experimental and numerical studies on amorphous systems. Chapter two has description of homemade experimental setup for carrying out our experiments on bubble rafts. In chapter three, we have shown that binary amorphous rafts show yielding. We have connected this yielding behaviour to non-affine microscopic events called T1 events. Temporal evolution of these non-affine events is studied and observed to saturate to a steady state value which is dependent on the applied strain amplitude. This steady state value which is dependent on applied strain amplitude serves as an order parameter and a relaxation time obtained from the temporal evolution of number of non-affine events characterise an absorbing phase transition at a critical strain associated with yielding in our system. Interestingly, within the experimental certainty, we have observed a roughening transition at a critical strain which coincides with the yielding.

This thesis consists of three chapters. First chapter gives an introduction to structural glasses and sheared glasses. We have also motivated our work with experimental and numerical studies on amorphous systems. Chapter two has description of homemade experimental setup for carrying out our experiments on bubble rafts. In chapter three, we have shown that binary amorphous rafts show yielding. We have connected this yielding behaviour to non-affine microscopic events called T1 events. Temporal evolution of these non-

affine events is studied and observed to saturate to a steady state value which is dependent on the applied strain amplitude. These steady state value which is dependent on applied strain amplitude serves as an order parameter and a relaxation time obtained from the temporal evolution of number of non-affine events characterise an absorbing phase transition at a critical strain associated with yielding in our system. Interestingly, within the experimental certainty, we have observed a roughening transition at a critical strain which coincides with the yielding.

Contents

Preface	vii
1 Introduction	<u>1</u>
1.1 Structural Glasses and Glass Transition	1
1.2 Glasses under Shear	1
1.3 Bubbles rafts as Soft Matter	3
1.4 Shearing bubble rafts	5
1.4.1 Fluctuations in static stress field	10
1.4.2 Understanding Shear-banding instability	12
1.4.3 Fluctuations in dynamic stress field	12
1.5 Foam flow as a Self-Organised criticality	14
1.6 Background and motivation for the present work	14
1.6.1 Chaotic dynamics in sheared suspensions	14
1.6.2 Random organisation in periodically driven systems	18
1.6.3 Simulations of irreversibility and Chaos in amorphous systems	21
1.6.4 Athermal glass under oscillatory shear	22
1.6.5 Experimental evidence for phase transition near yielding . . .	26
2 Experimental Section	<u>31</u>

2.1	Interfacial Rheology	31
2.1.1	Shear measurements at constant area	33
2.1.2	Interfacial Rheometer	33
2.2	Experimental Setup	35
2.2.1	Stability of the raft	35
2.2.2	Steps describing how we arrived at the setup	36
2.3	Oscillatory Rheology	37
2.4	Image processing	39
3	Yielding and onset of irreversibility in athermal amorphous rafts	<u>43</u>
3.1	Measurement of yield strain	43
3.2	Microstructural changes accompanying yielding	44
3.2.1	Algorithm to obtain T1 events	45
3.2.2	Irreversible T1 events	47
3.2.3	Steady state Irreversible T1 events as order parameter	48
3.3	Interface fluctuations	53
3.4	Steady state measurements of G' and G''	56
3.5	Conclusion	59
3.6	Future of our experiments	61
	References	<u>63</u>

CHAPTER 1

INTRODUCTION

1.1 Structural Glasses and Glass Transition

Structural glasses are widely used in material and aerospace industry. Glasses with desirable mechanical and optical properties can be designed according to the microscopic understanding of the glassy state which remains a challenge for condensed matter physicists[1; 2]. While glasses are mechanically rigid like that of crystalline solids, their microstructure is analogous to a liquid. Since rigidity is associated with broken translational symmetry, it remains a challenge to explain the rigidity of the glassy state. Upon cooling a liquid, molecular dynamics slows down and if cooled slowly across its freezing temperature T_m , it adapts to a crystalline state which is a first order transition[3]. But on cooling rapidly molecules do not have sufficient time for rearrangements and the system appears frozen on the experimental time scale. The temperature below which this state is achieved is the glass transition temperature T_g [4]. This description is represented graphically in Figure 1.1 which shows the temperature dependence of liquid's volume at constant pressure.

1.2 Glasses under Shear

Deformation in crystalline materials is characterised by dislocations present in them[5]. When a shear stress is applied to the material as shown in Figure 1.2, it

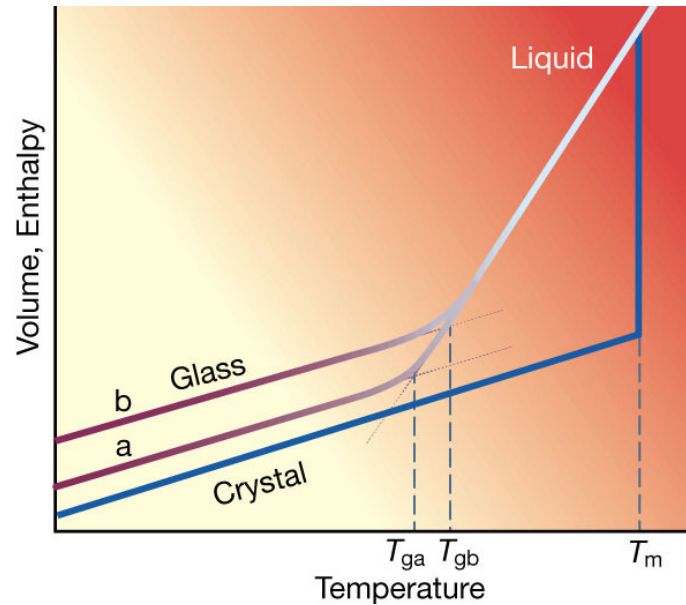


Figure 1.1: Temperature dependence of a liquid's volume V or enthalpy H at constant pressure. T_m is the melting temperature. A slow cooling rate gives a glass transition at T_{ga} ; faster cooling rate produces a glass transition at T_{gb} . Adapted from[4].

deforms along the slip plane by means of dislocation motion. Amorphous systems do not have any topological order and at present the deformation mechanisms for glasses remain unclear.

The study of deformation and flow of amorphous materials/glasses can answer questions related to efficient mechanical properties of glasses. Be it amorphous or crystalline solid, the deformation has to involve structural rearrangements[6]. However, the length scales at which these happen are too small and time scales are too short in atomic systems.

Soft matter systems are ideal to study the dynamics of glassy state at observable time and length scales experimentally. Colloidal assemblies[7], emulsions, foams, and also granular matter are different soft matter systems and can exhibit glassy behaviour. Deformation and flow (rheology) of these complex fluids is a fascinating phenomena because they are viscoelastic - they have mechanical properties

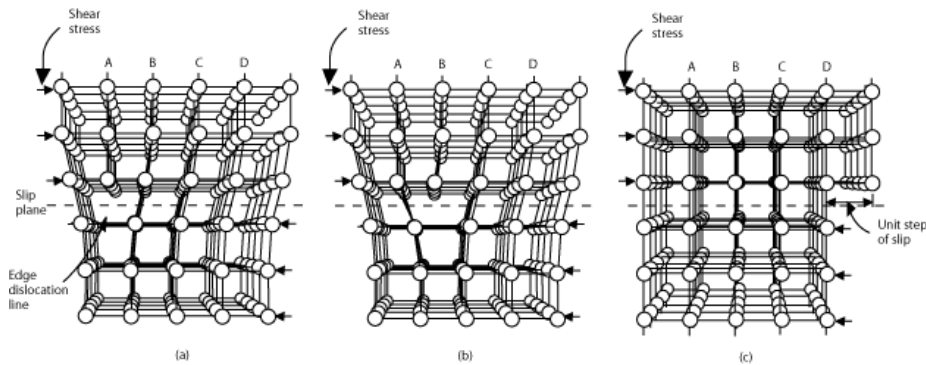


Figure 1.2: Arrows show the direction of applied stress; Dislocation motion is showed from (a) -(c); in (c) unit step of slip is shown. Adapted from google images.

in between elastic solids and viscous liquids[8]. Direct real space visualization of microstructural rearrangements can be possible with sheared colloidal systems[9]. Results from numerous experiments on sheared colloidal systems have shown that microstructural dynamics of amorphous systems show yielding at a critical shear strain([10; 11]). Colloidal systems are thermal as they diffuse and exhibit Brownian motion. But what is the case for systems where there is no role of temperature i.e., in the limit thermal fluctuations are zero? How are the microstructural dynamics and rheology of athermal glasses related? Argon and Kuo in 1979[12; 13] first proposed a model system for studying sheared athermal amorphous systems. Raft consisting of particles of two different sizes roughly in equal numbers forms amorphous system and has structural characteristics of metallic glass.

1.3 Bubbles rafts as Soft Matter

Bubble rafts are dispersions of gas bubbles in surfactant solution at air liquid interface. The size of each bubble is 1 mm to 1 cm and thickness of the liquid films separating neighbouring bubbles is generally between 10 nm to a few μ m. Every bubble of the raft is considered as an atom as capillary forces between the bubbles

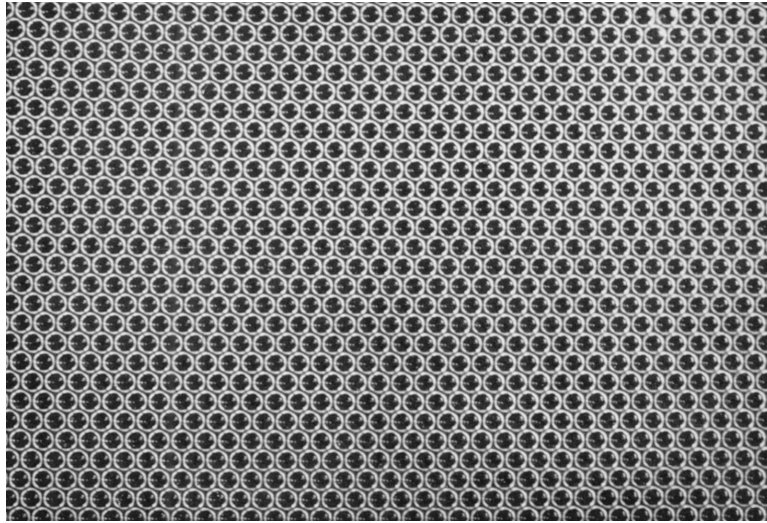


Figure 1.3: Bubble raft showing hexagonal packing in 2 dimensions. Adapted from [14].

are analogous to interatomic forces that are used to model atomic systems[14][15], Figure 1.3. They resemble other complex systems such as emulsions, gels and vesicles. These systems show yielding at the cross-over of solid-like and liquid-like behaviours, jamming and slow relaxation dynamics characterizing soft glassy rheological behaviour[16]. These mesoscale systems are easy to track using video microscopy and microscopical physical phenomena can be studied elegantly.

Bubble rafts and granular systems are soft systems in zero temperature limit and hence are athermal systems. They both share many similar characteristics. But in contrast, the grains of granular systems are incompressible, and pack at packing fractions below random close packing (84% for 2D systems and 63% for 3D systems), while bubbles of the raft can readily deform and squashed together and pack above random close packing. Also grains of granular systems are subjected to static and sliding friction as well as to collisions, whereas bubble contacts are through a liquid film that typically do not support static friction. These simplify

the interpretation of deformation in bubble rafts and is the subject of focus for the remaining part of this thesis.

1.4 Shearing bubble rafts

As described in previous section, in molecular glasses, structural relaxation on approaching T_g is due to activated thermal motion and results in aging. In case of foams, the thermal energy is zero and non-thermal effects like coarsening, coalescence and drainage describe aging process. When bubble raft is subjected to a steady shear, at high strain rate it behave like a Herschel-Bulkley[17] fluid and in the limit of zero strain it exhibits a bifurcation in viscosity[18] and a time evolution in viscosity[19]. Under oscillatory shear, for small strain amplitudes they behave predominantly like elastic solids and for large strains they behave predominantly like viscous liquids with viscosity that decreases with shear rate (shear thinning). Oscillatory rheology allows one to probe quasistatic elastic response of the system by increasing the driving frequency. Unlike polycrystalline materials, when shear stress is applied, they undergo change in shape due to sharp shear translation between adjacent close packed rows in the raft. Shear translation is the result of stress relaxation and these stress relaxing regions are termed as Shear Transformation Zones (STZ), Figure 1.4. The term STZ is first coined by Ali Argon to explain metallic glass deformation[12]. In these STZs due to absence of long range order, topological rearrangements named as T1 events and T2 events occur.

Bubble raft when sheared, stores elastic energy in the form of bubble deformations and then system subsequently relaxes through bubble rearrangements. These topological events that results in stress drop in the system stochastically are T1 events. T1 event is a neighbour switching among four particles as shown in Figure

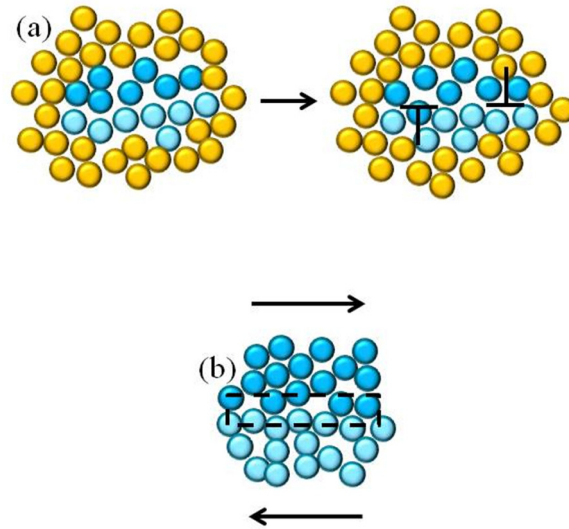


Figure 1.4: (a) A shear transformation zone visualized as a nanoscopic dislocation loop. Under stress, the top half of the blue atoms shift with respect to the bottom half, but the surrounding disordered yellow atoms prevent the displacement from propagating beyond a distance of 1-2 nm. (b) Only blue atoms from (a) are shown with two different set of close packed rows. Adapted from [12].

1.5. In configuration-1 particles labelled 1, 2 are nearest neighbours and particles labelled 3, 4 are next nearest neighbours. When a steady shear is applied on to the system, particles labelled 3, 4 become nearest neighbours and particles labelled 1, 2 become next nearest neighbours as shown in configuration-2. The change in configuration from 1 to 2 accounts for one T1 event. In case when an oscillatory shear is applied to the system, two possibilities arise. One, at the end of a cycle configuration-1 goes to configuration-2 and returns back to configuration-1 which is a reversible T1 event or an affine transformation and system retains its original configuration. Second, at the end of a cycle configuration-1 goes to configuration-2 and to configuration-3 which is an irreversible T1 event or a non-affine transformation and system attains new configuration. Number of irreversible T1 events is characteristic of plastic deformation in amorphous systems. Diffusive wave microscopy was used to detect T1 events in 3D foams directly[20][21][22][23]. But

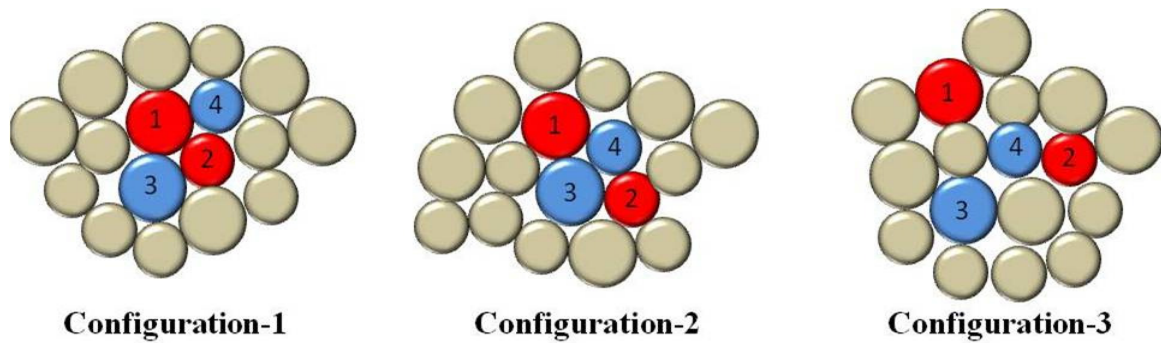


Figure 1.5: T1 event among four particles of an amorphous system when sheared. Configuration-1 to Configuration-2 is a reversible T1 event. Configuration-1 to Configuration-3 is an irreversible T1 event.

this technique does not provide good spatial resolution because of which rheological measurements on foams are now focused on 2D systems.

Mechanical deformation of 2D foams have been rigorously studied both numerically [23][24][25][26][27][28] and experimentally[29][30][31][32]. Bubble rafts when sheared in a Couette geometry, due to zero velocity at the no slip boundary (at the rim), the velocity profile resembles a plug flow as shown in the Figure 1.6[33] for different shear rates. It was also shown that the viscosity liquid layer that is present between two bubbles plays an important role in studying dynamics beyond yield point where foam behaves like a viscous fluid[23]. When amorphous systems are subjected to small deformation, they follow deformation induced continuous changes in the local minimum. hence every particle tracks energy local minimum. Within the elastic limit, particle returns to its original position after every cycle as shown in Figure 1.7, reversible elastic step[34]. With increase in shear strain/deformation, chance of returning back to the original position decreases as shown in Figure 1.7, irreversible plastic step.

When a viscoelastic solid is sheared with strain, $\gamma(t) = \gamma_o \sin(\omega t)$, steady state

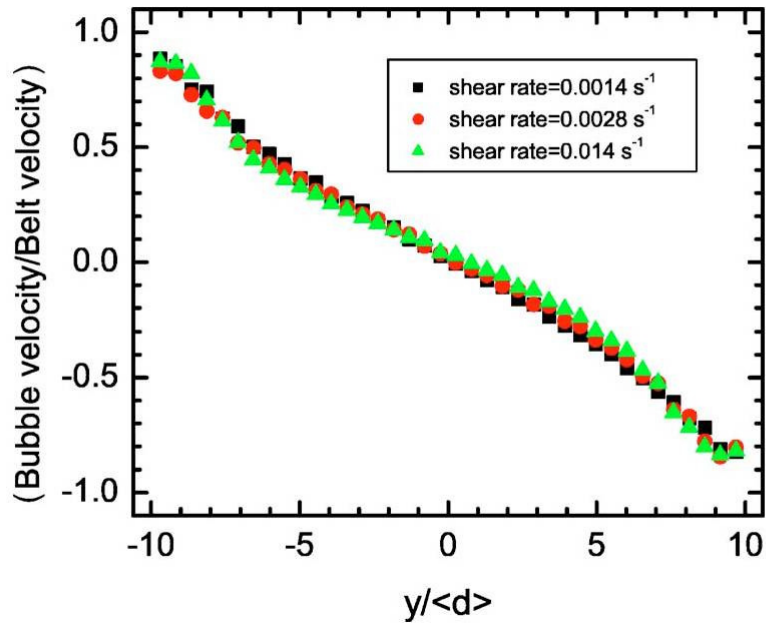


Figure 1.6: The scaled velocity profile as a function of scaled position ($y/\langle d \rangle$) for three different rates of strain for a system with Couette geometry, where $\langle d \rangle$ is the average bubble diameter. Adapted from [33]

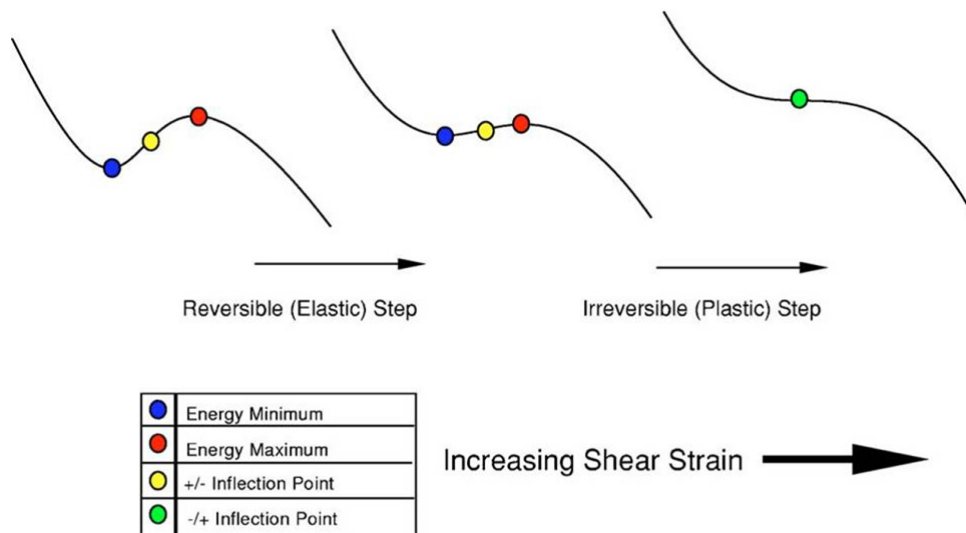


Figure 1.7: A schematic representation of deformation-induced changes of a local minimum in the potential energy landscape. The shape of the landscape varies continuously as the strain is increased going from left to right with both the location and height of the minimum changing. Adapted from [34]

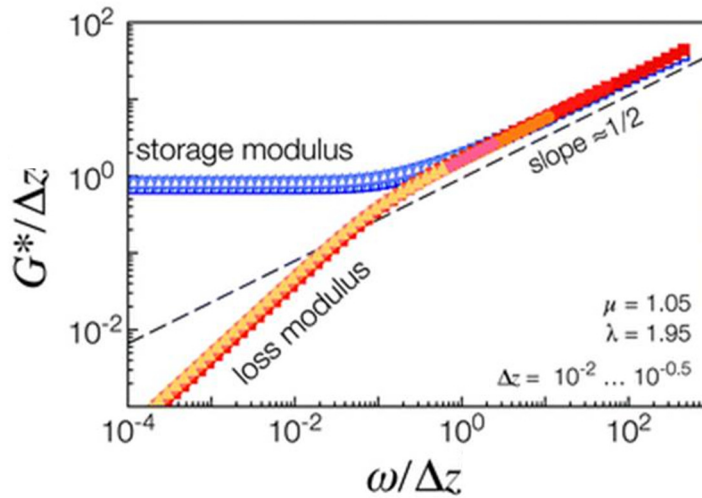


Figure 1.8: Numerically computed storage modulus G' (open symbols) and loss modulus G'' (filled symbols) rescaled with varying distance to jamming Δz (legend). Adapted from [35]

stress is also sinusoidal and has both in-phase (elastic/Storage component) and out-of-phase (viscous/loss components) contributions, $\sigma(t)/\gamma_o = G'(\omega)\sin(\omega t) + G''(\omega)\cos(\omega t)$. These two components together define frequency dependent complex shear modulus, $G^* = G' + iG''$. In a slowly sheared viscoelastic solid, G' approaches quasistatic shear modulus G_o . Also $G'' = \eta_o\omega$ is linear in frequency (Newtonian) where η_o is the dynamic viscosity. Figure 1.8 shows numerically computed elastic and viscous moduli from bubble raft model[35]

Rheological measurements of 2D foams using oscillatory strain were well studied by Kabala and Debregeas[36][37]. Numerically they have modelled quasi-two dimensional foam system which consists of monolayer of bubbles with two different sizes confined between two horizontal plates. Experimentally they have studied 2D foams under oscillatory shear. These systems are aimed to understand connections between mechanical properties and microstructure. Velocity flow profiles as described in earlier works can arise due to the geometrical constraint of the exper-

imental system (Couette geometry). So, simulation work has considered parallel plate geometry where shear stress is homogeneous and geometry does not play a role. Mechanical properties of the system are observed to evolve with time and this evolution is explained using evolution of shear bands. Shear bands are observed to evolve above a critical strain and tend to saturate. This is correlated with the increase number of non-affine rearrangements and their tendency to move to the side of moving plate. Stress versus strain plot, Figure 1.9(a) shows a linear increase showing the elastic behaviour of the system and for $\gamma_o \geq 1$ shear banding occurs and shear stress overshoots and saturates showing avalanche of rearrangements. Also number of T1 events are less and randomly distributed for $\gamma_o < 1$ and for $\gamma_o \geq 1$, T1 events gather in a narrow region close to the moving plate as shown in Figure 1.9(b). When T1 event occurs, it triggers an avalanche of events in the near neighbourhood region. A powerlaw decay of the avalanche size distribution is observed with an exponent of $-3/2$ which is close to mean field value. It is in agreement with the numerical studies of Chen, Bak and Obukhov(1991) and Okuzono and Kawasaki(1995) on elastic disordered systems. This suggests that the exponent value is generic feature of these systems.

1.4.1 Fluctuations in static stress field

To understand the spatial fluctuations of static stress field developed due to avalanche of T1 events, a section of the system which is radially symmetric and having a width of one bubble diameter is considered. To characterise these fluctuations, a quantity called bubble shear stress deviation defined for each bubble in this section as, $\delta_s \sigma_i = \sigma_i(t) - \langle \sigma(y, t) \rangle$ $\langle \sigma(y, t) \rangle$ is the mean shear stress in the

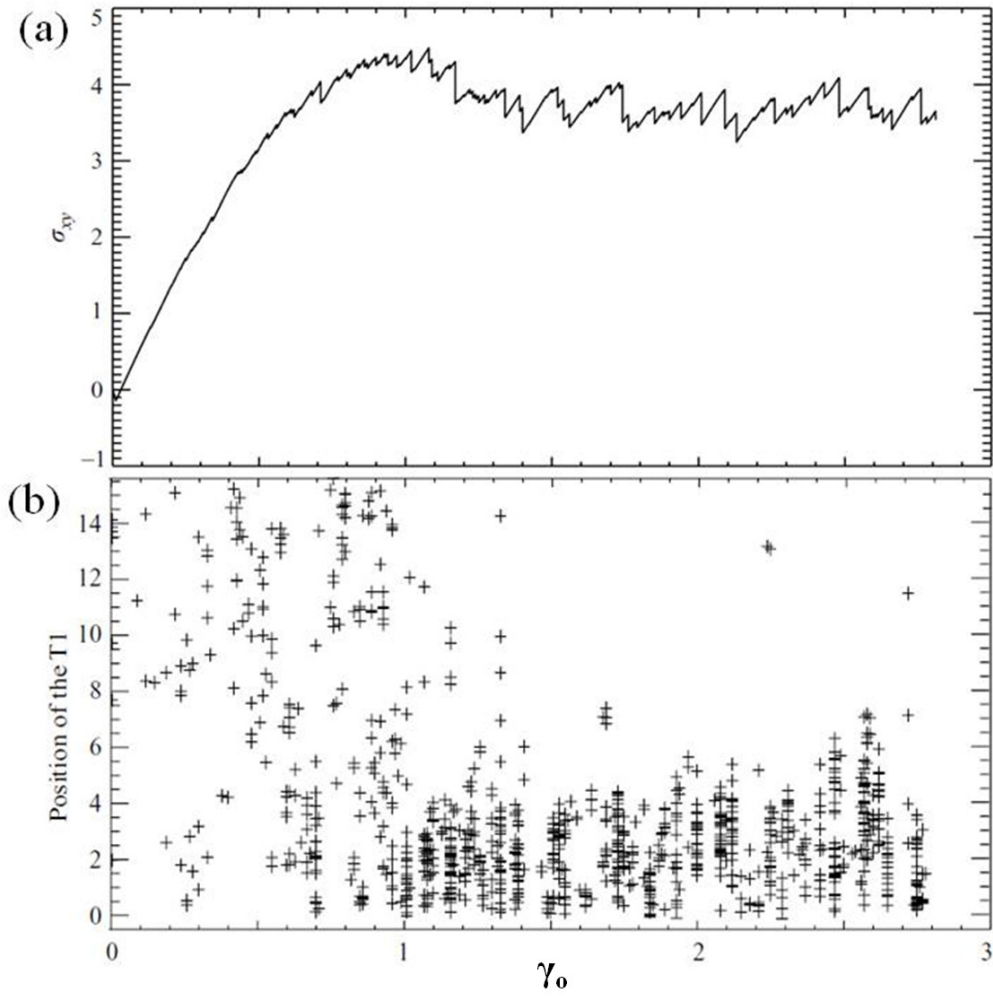


Figure 1.9: Evolutions of (a) the shear stress, (b) the positions of the T1 events within the gap (geometry) as a function of the applied strain (data from the simulation). Adopted from [37]

corresponding section. Figure 1.10 shows the distribution of bubble shear stress in both experiment and simulation at shear band and region located 10 particle diameters from shear band. Variance of these plots is wider at the location of shear band than in other regions.

1.4.2 Understanding Shear-banding instability

Wider is the variance of stress distribution, greater is the probability of finding clusters of bubbles subjected to large strains. These regions are more likely to yield plastically with increase in shear stress. Therefore it is reasonable to associate wider variance of stress distribution to decrease in the yield stress. To explain this assumption, two distinct regions of the foam are considered whose initial stress distributions are same. With the increase in mean shear stress, T1 events start appearing and trigger an avalanche of rearrangements. This triggering breaks the symmetry of the system which results in onset of shear-banding.

1.4.3 Fluctuations in dynamic stress field

Dynamic shear stress deformation for each bubble for a section of raft (as described earlier) is given as, $\delta_d\sigma_i(t, \Delta t) = \delta_s\sigma_i(t + \Delta t) - \delta_s\sigma_i(t)$. In the same way as static stress distribution, variance of dynamic stress distribution decreases on moving away from shear band and the decrease is more pronounced. Thus, shear-band instability helps in understanding the two regimes of mechanical response of glass when subjected to a mechanical deformation (shear strain).

As fundamental problem in the physics of amorphous materials/structural glasses is to understand reversible elastic behaviour to irreversible plastic behaviour and its connections to yielding, above described approaches can provide more insights

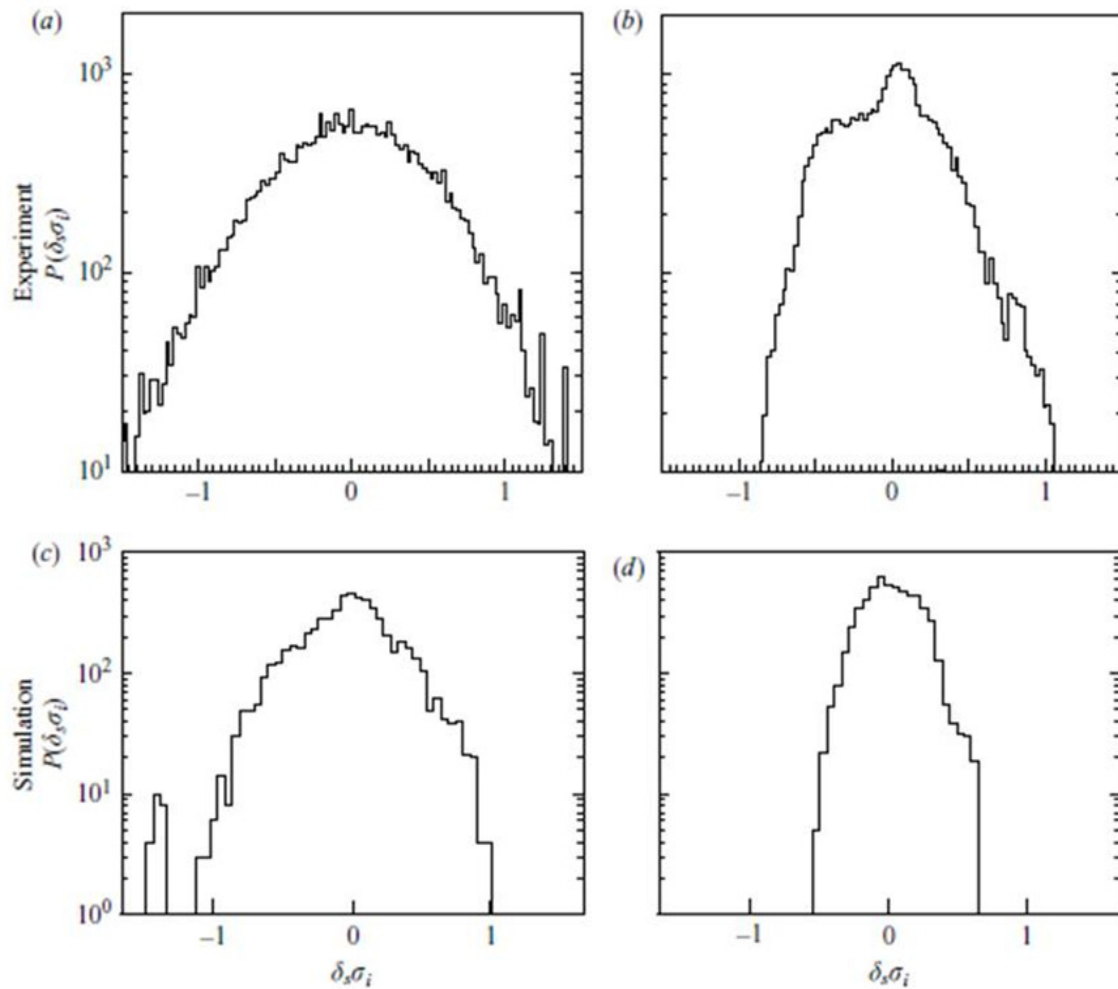


Figure 1.10: Distribution of the bubble shear stress deviation $\delta_s \sigma_i$ to the local mean value (a, b) in the experiment and (c, d) in the simulation, in the steady-state regime. Two different regions are analysed: (a, c) the shear band, and (b, d) a region located 10 bubble diameters away from the shear band. The regions correspond to strips of width 1 bubble diameter in the experiment, and 2 bubble diameters in the simulation. Adopted from [37]

into understanding of microstructural relaxations in structural glasses.

1.5 Foam flow as a Self-Organised criticality

The dynamics and rheology of foams can be understood using the concept of self-organised criticality[38]. Vertices of cellular patterns of foams are considered to model the system and mechanical properties are calculated. The dynamical behaviour of the system has similarities with stick-slip process of earthquake models that exhibit self organised criticality. So the time series analysis of interfacial energy, $E(t)$ and average stress tensor, $\tau_{xy}(t)$ was analysed and power spectrum for both of the quantities are defined probability density of avalanche sizes, $P(s)$ for $E(t)$ and $P(s')$ for $\tau_{xy}(t)$ are plotted as shown in the Figure 1.12 and Figure 1.13. Avalanche size is defined as the total energy density for an avalanche. Both $P(s)$ and $P(s')$ show power-law behaviour $P(s) \sim s^{1-\tau}$ and $P(s') \sim s'^{1-\tau}$ with almost same exponents. τ is close to mean-field value $5/2$ for sandpile model. Hence there is a possibility that rheological behaviour of 2D foams can be understood using the concept of self-organised criticality which explains the time evolution of mechanical properties[39].

1.6 Background and motivation for the present work

1.6.1 Chaotic dynamics in sheared suspensions

A Newtonian fluid at low Reynolds number, Re when sheared between two concentric cylinders also known as circular Couette flow, is time reversible. This behaviour is consistent with the reversibility of Stokes equations or creeping flow

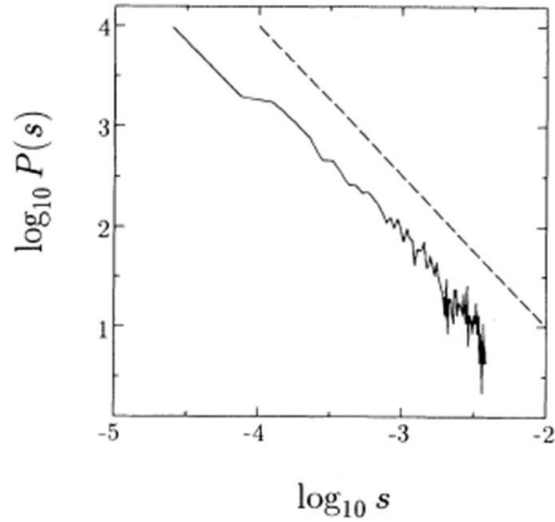


Figure 1.11: Doubly logarithmic plot of the probability density $P(s)$ of the avalanche size appears to obey a power law. The dashed line has the slope $-\frac{3}{2}$, which is the mean-field value. Adopted from [38]

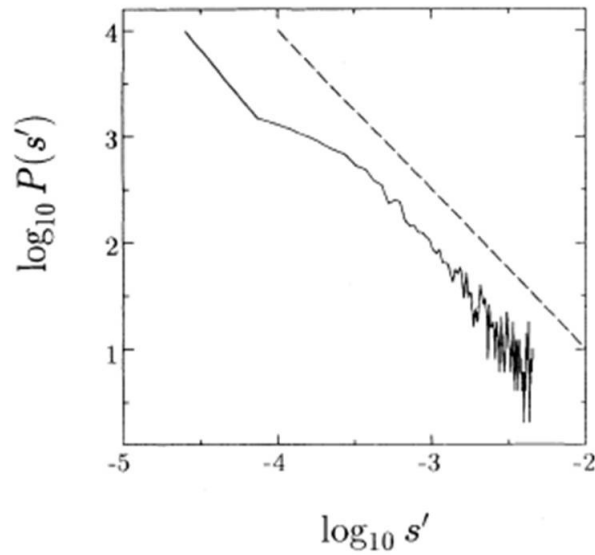


Figure 1.12: Doubly logarithmic plot of the probability density $P(s')$ of the stress jump in an avalanche appears to obey a power law with almost the same exponent as that of $P(s)$. The dashed line has the slope $-\frac{3}{2}$. Adopted from [38]

equations which govern low Re behaviour of non-brownian suspensions. In order to demonstrate this, consider three particles falling through a viscous liquid. If the trajectories of each particle is tracked in time, and compared with respect to the other, they are observed to be chaotic[40] as explained by Taylor[41]. Hence, chaos is an intrinsic property of sheared non-brownian suspensions at low Re . Mean squared displacements ($MSDs$) for such systems is studied and is as shown in Figure 1.13[42], one along shear direction and other in perpendicular direction to the shear. $MSDs$ are linear in time and are of different magnitude in the two directions. This anisotropy induced by the shear flow in the system is a consequence of Taylor dispersion[43]. Diffusivities calculated from $MSDs$ are as shown in Figure 1.14 in the numerical study and experiment on a similar system. Upon shearing above a critical strain, there is a rapid onset of irreversibility in the system. This irreversibility can be understood by computing the time evolution of phase space trajectories of two nearby particles. Separation between these trajectories, $\delta(t)$ is observed to increase exponentially in time characterised by Lyapunov exponent, λ [42]. Figure 1.15 shows the increase in the positive Lyapunov exponent as a function of strain. Increase in positive λ signifies chaotic nature of the system. Thus irreversible behaviour in the particle dynamics observed in [42] is due to chaotic nature of hydrodynamic interactions between the suspensions of non-brownian particles. But what happens to the dynamics of the similar systems when oscillatory shear is applied? This question was answered by Pine et al., through an experimental study.

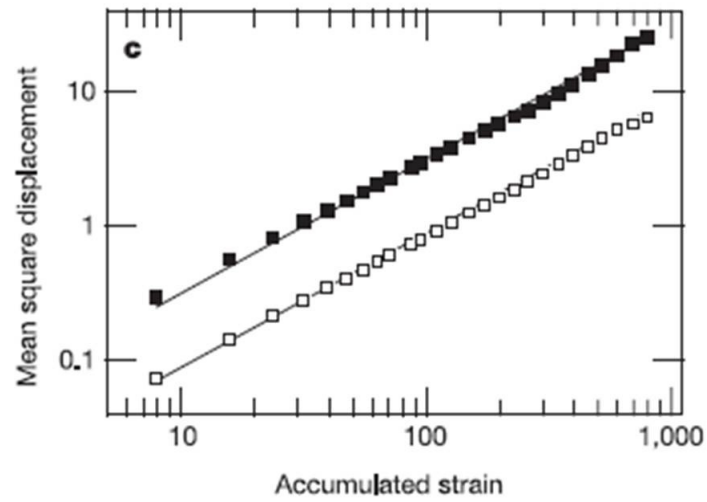


Figure 1.13: The filled and open squares are the mean square displacements $\langle x^2 \rangle$ and $\langle z^2 \rangle$ respectively. Adopted from [42]

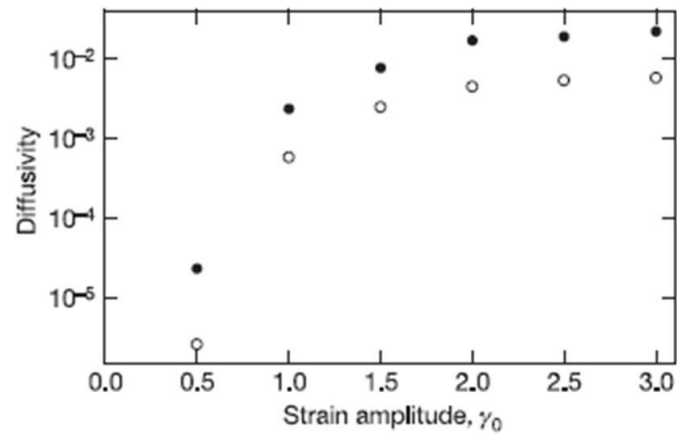


Figure 1.14: Experimental effective diffusivities D_x (filled circles) and D_z (open circles) as a function of the oscillatory strain amplitude, on a logarithmic scale for volume fraction $\phi = 0.40$. Adopted from [42]

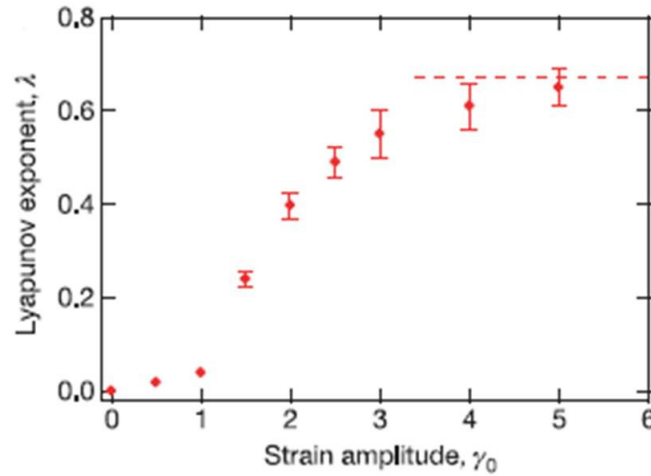


Figure 1.15: Numerically computed Lyapunov exponent λ versus strain amplitude γ_0 . Adopted from [42]

1.6.2 Random organisation in periodically driven systems

Experimental system used by Pine et al., consists of a Taylor-couette cell filled with viscous liquid ($Re \rightarrow 0$) into which density and index matched particles are loaded (30% volume fraction). Then inner cylinder is then rotated back and forth with different amplitudes, amplitudes. It is observed that at small amplitudes, trajectories are reversible and particles return back virtually to the initial position. But at large amplitudes particles do not return to their original position and trajectories are irreversible. This imply there is a sharp transition from reversible to irreversible behaviour with increase in amplitude of rotation. In order to understand this transition, they have performed experimental and numerical study on non-brownian suspensions driven periodically.

Figure 1.6 (a, b)[44] shows the system of 2D non-brownian particle suspension for an area fraction $\phi = 0.2$ subjected to oscillatory strain amplitudes, 3,2. Filled circles represent active particles. In both the cases, initial configuration is random

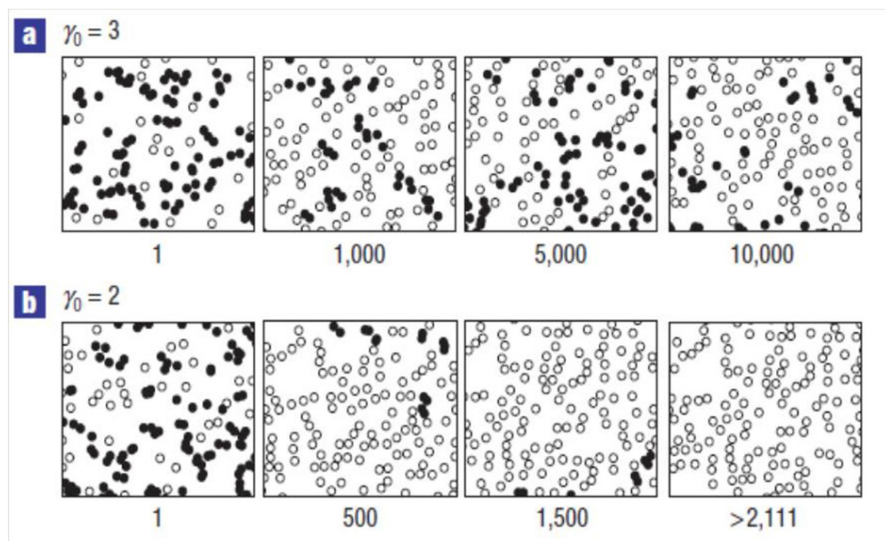


Figure 1.16: Simulation results for the 2D model, showing particle activity above and below the strain threshold as a function of number of shear cycles. (a) (b) are snapshots of the particle distributions for two strain amplitudes 3.0 and 2.0, for area fraction 0.2 and particle number 1,000. Filled black circles indicate particles that are active and thus be irreversibly displaced in the next shear cycle; open circles indicate particles that are reversible. The shear flow direction is horizontal.. Adopted from [44]

and when sheared, generates many collisions in the initial shear cycles. These two suspensions are subjected to constant oscillatory strains, $\gamma_o = 3$ for Figure 1.6 (a) and $\gamma_o = 2$ for Figure 1.6 (b). These are observed to evolve in time. After few hundreds of cycles, for $\gamma_o = 2$, configuration in Figure 1.6 (b) evolves to an steady state where there are no active particles and is termed as absorbing steady state. For $\gamma_o = 3$, configuration in Figure 1.6 (a) evolves to a steady state where there are finite number of active particles and is termed as fluctuating steady state. Recent studies have shown that non-equilibrium systems can undergo a phase transition from fluctuating dynamical steady state into an absorbing state[45]. These transitions have signatures of critical phase transition.

Number of active particles in both the cases, $\gamma_o = 3$ and $\gamma_o = 2$ is plotted as a

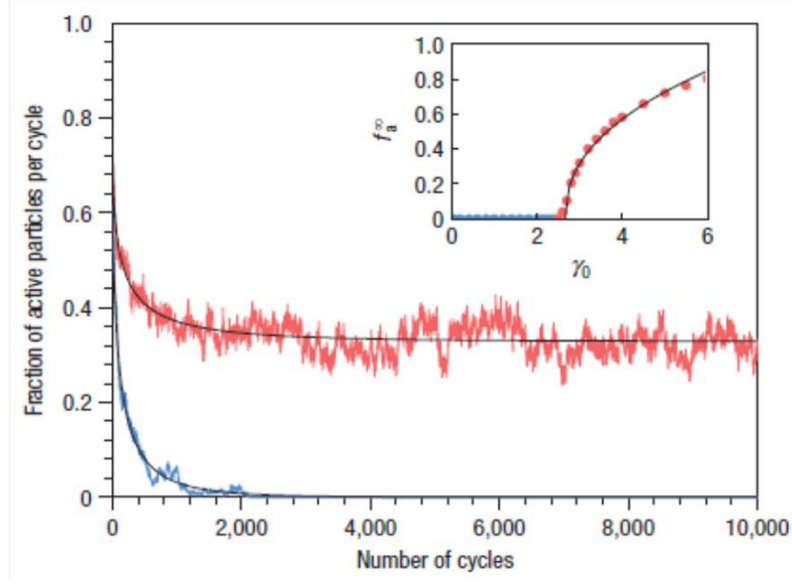


Figure 1.17: Fraction of active particles per cycle f_a as a function of number of shear cycles for the two different strain amplitudes, 3.0 (red) and 2.0 (blue). Inset: Fraction of active particles in steady state as a function of strain amplitude. Adopted from [44]

function of number of cycles in Figure 1.17. These relaxation curves are fitted to the function form, $f_a(t) = (f_a^0 - f_a^\infty) \frac{e^{-t/\tau}}{t^\beta} + f_a^\infty$, f_a^0 and f_a^∞ are respectively initial and steady state values of f_a . $f_a(t)$ exhibits a crossover from exponential to power-law behaviour as critical phase transition. Fraction of active particles in steady state is plotted as a function of number of cycles and is observed to be zero below critical strain and tend to increase above it. Hence there is a clear transition from absorbing state to fluctuating steady state. Hence, steady state active fraction serves as an order parameter and above the critical strain it can be fitted to $f_a^\infty \sim (\gamma_0 - \gamma_0^c)^\beta$, with $\beta = 0.450.02$

The characteristic time τ taken for the system to reach steady state is obtained from functional form fit to fraction of active particles and plotted as a function of active particle number as shown in Figure 1.18. Divergence is observed at the same critical strain amplitude as that of active particle fraction and this follows a

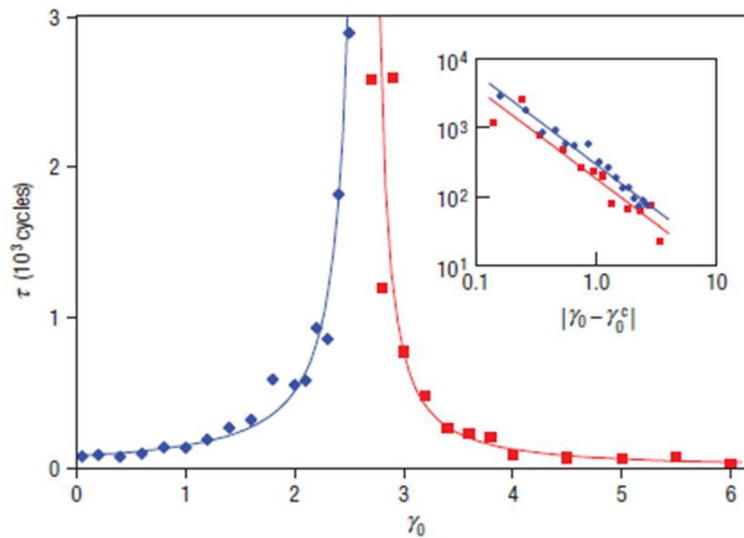


Figure 1.18: Simulation results for the characteristic time τ to reach steady state as a function of the strain amplitude γ_0 for an area fraction of $\phi = 0.20$ and 1,000 particles. Blue symbols, below transition ($\gamma_0 < \gamma_0^c$); red symbols, above transition ($\gamma_0 > \gamma_0^c$). Adopted from [44]

power-law above the critical strain given by, $\tau = |\gamma_0 - \gamma_0^c|^{-\nu}$, with $\nu = 1.33 \pm 0.02$.

1.6.3 Simulations of irreversibility and Chaos in amorphous systems

For dilute suspensions of non-brownian particles, a critical phase transition is observed from an absorbing steady state to fluctuating steady state. Also, chaotic nature is observed in their dynamics. What is the case if dense systems are considered? Unlike dilute suspensions, dense amorphous systems rearrange their positions in a non-trivial manner causing non-affine deformations whose displacement field is quadrupolar as discussed above in section- 1.2.

Amorphous systems under periodic shear have been studied numerically[46].

For small strain amplitudes after certain number of cycles, material becomes completely repetitive. This is observed from potential energy per particle site as a function of accumulated strain. With increase in strain amplitude, above a certain critical strain, system does not reach a stable limit cycle. For such systems, time taken to reach stable limit cycle can be obtained from cycle decorrelation function for potential energy of the system, $R(n) = \int |U(t, n) - U(t, n - p)| dt$. This function reaches zero after certain number of cycles (depending on the strain) for small strain amplitudes. But for larger strain amplitudes, the function relaxes to some asymptotic finite value. Figure 1.19 shows $R(n)$ as a function of cycle number, n . Figure 1.20 shows the relaxation time, time taken by $R(n)$ to reach below 1% of its initial value. This parameter follows a power law with critical strain as $\gamma_c = 0.11$. This critical strain is close to yield strain as shown in Figure 1.21. Again in this case, the increase in positive lyapunov exponent above yield strain corresponds to transition to chaos.

1.6.4 Athermal glass under oscillatory shear

Many computational studies have been carried out to understand behaviour of amorphous systems at zero temperature. 3D binary Lennard-Jones model is used to model athermal systems for numerical simulations[47]. When these systems are sheared, for low strain amplitudes, system reaches non diffusive state retaining memory of initial conditions. When sheared at high strain amplitudes, they are diffusive characterised by diffusion coefficient and are independent of initial conditions. Because oscillatory strain is applied, at the end of every cycle, particle attains a configuration with $\gamma = 0$ which are called zero strain configurations. Average potential energy per particle in zero strain configuration is plotted as a function

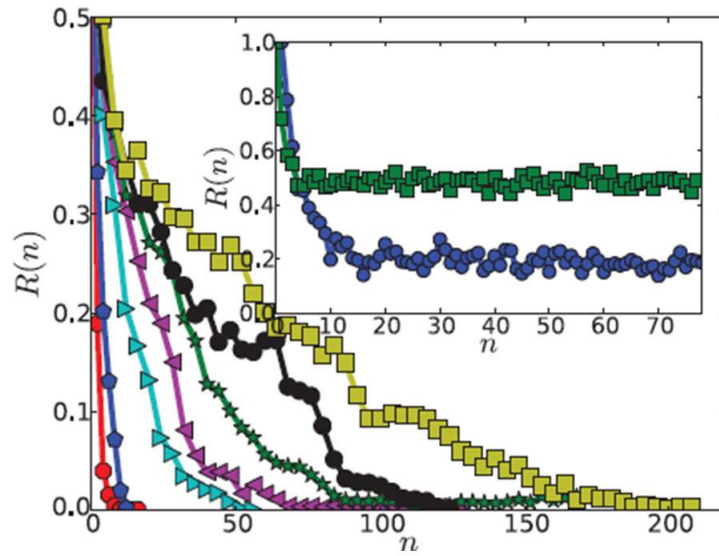


Figure 1.19: Cycle decorrelation function as a function of the number of cycles, for system size $N = 16384$ particles for strain amplitudes $\gamma = 0.06, 0.07, 0.75, 0.85, 0.88, 0.09, 0.093,$ and 0.095 (from left to right). Inset: The same function for strain amplitudes $\gamma = 0.12$ (blue circles) and $\gamma = 0.15$ (green rectangles). Adopted from [46]

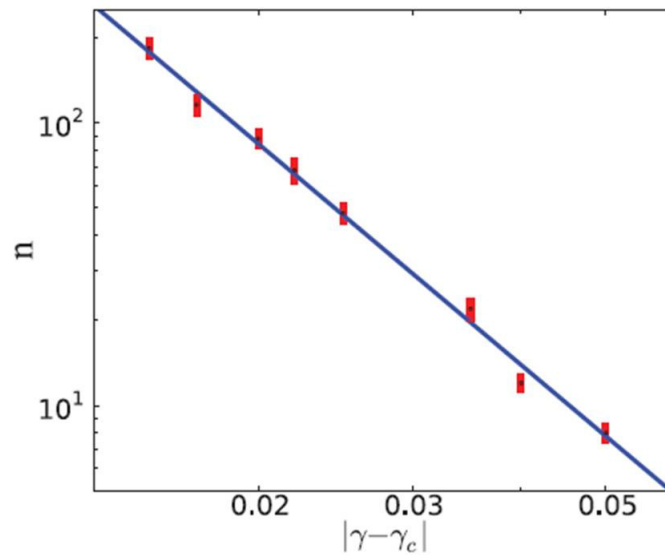


Figure 1.20: Log-log plot of the typical number of cycles n before reaching periodic behaviour as a function of the strain amplitude γ . Adopted from [46]

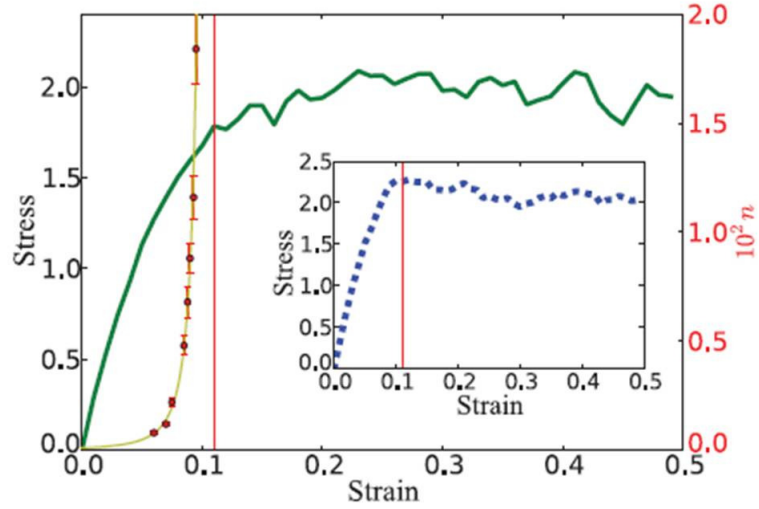


Figure 1.21: Stress-strain curve from molecular dynamics simulations for 16 384 particles under quasistatic shear. Red dots represent the number of cycles, n , required to reach periodic behaviour under oscillatory shear (the scale is on the right side of the figure in red). The vertical red line is the strain amplitude for which the time to reach reversible behavior diverges. Inset: stress-strain behaviour for the same parameters as the solid green curve but with different initial particle configurations the vertical red line is the same as in the main figure. Adopted from [46]

of accumulated strain γ_{acc} , as shown in Figure 1.22. These curves are fitted to a stretched exponential and a characteristic relaxation strain γ_{acc}^c is extracted. γ_{max} is the maximum amplitude of strain oscillation cycle. Figure 1.23 shows γ_{acc}^c as a function of γ_{max} . This plot resembles active particle fraction as a function of cycle number in [44]. $MSDs$ obtained for particles at small strains, tend to saturate where as for large strains it is diffusive. Diffusivity D extracted from MSD is zero below a critical strain, γ_c and increases rapidly as shown in Figure 1.24. Above critical strain this can be fitted to a power law and exponents are obtained depending on γ_c . Stress strain curves for this system shows a hysteresis and hysteresis area increases with increase in γ_{max} .

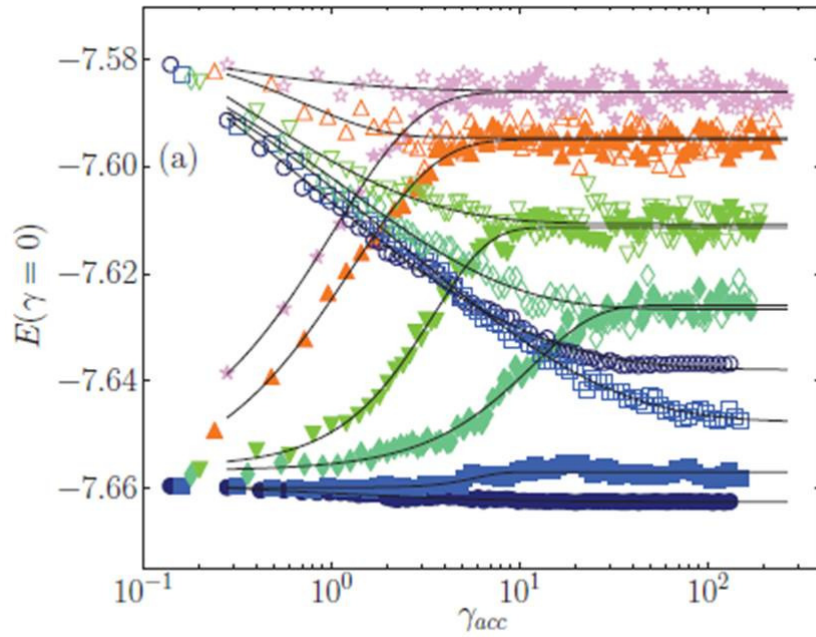


Figure 1.22: Potential energy per particle E for zero-strain configurations, for different values of γ_{max} averaged over different runs with samples of $N = 4000$ particles at $T = 0.466$ (closed symbols) and $T = 1.0$ (open symbols). Adopted from [47]

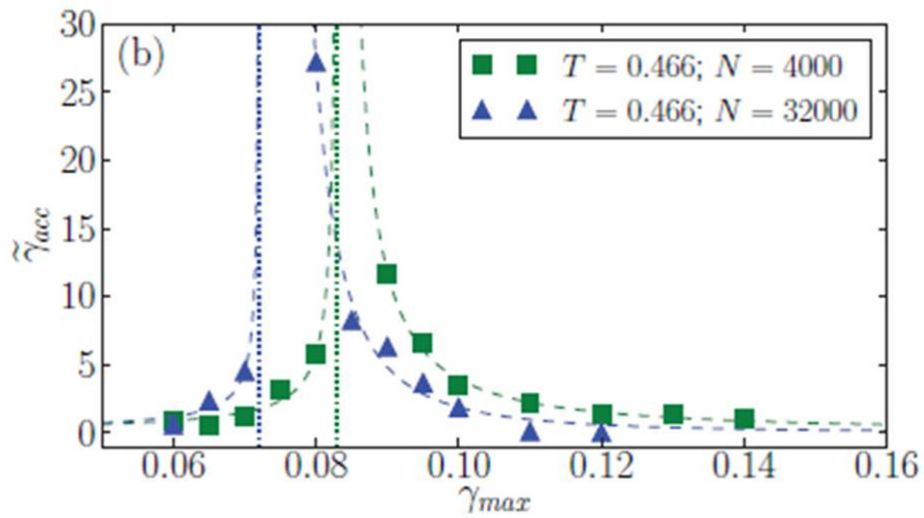


Figure 1.23: $\tilde{\gamma}_{acc}^c$ as a function of γ_{max} . Adopted from [47]

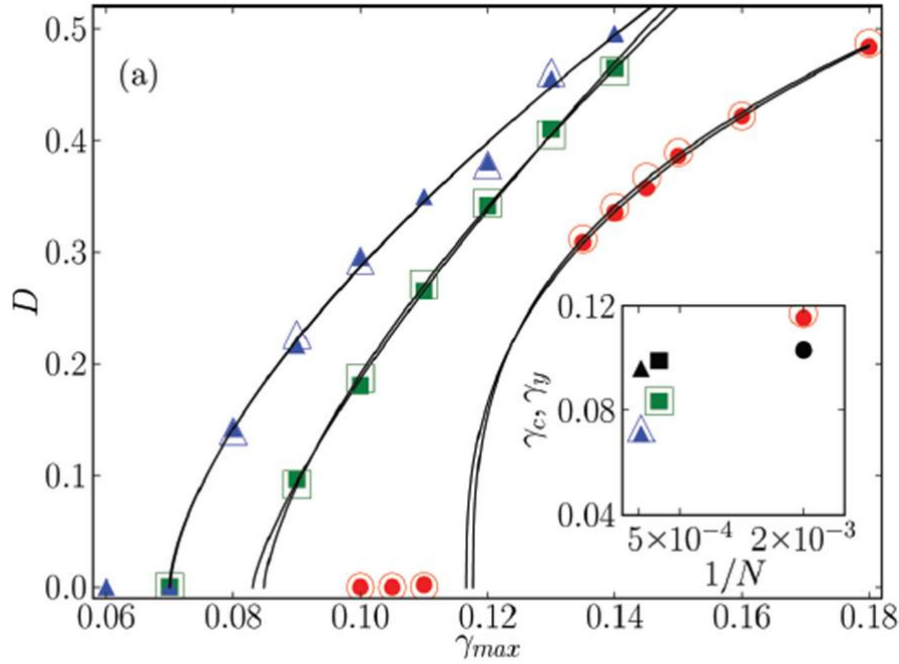


Figure 1.24: Diffusivity D extracted from MSD by fitted to a power law as a function of γ_{max} . Inset: γ_c vs inverse system size $1/N$. Adopted from [47]

1.6.5 Experimental evidence for phase transition near yielding

Rheological studies of soft systems give insight into their mechanical response. Relationship between microstructure and rheological response was studied by Keim and Arratia by carrying out interfacial rheology of soft particles[48]. As described above, amorphous systems, when sheared undergo structural rearrangements quantified by T1(non affine) events. Net number of irreversible T1 events plotted as a function of accumulated strain, $\gamma_{acc} - 4N\gamma_o$ where $N = \text{Cycle number}$ is as shown in Figure 1.25. From the plot it is evident that there is a critical strain below which system evolves to a reversible state signified by the T1 event number saturating to zero. At large strain amplitudes (above a critical strain), it saturates roughly to a constant number. This result is supported by steady state oscillatory rheology of the bulk material measured in the same experiment simultaneously. Elastic storage

modulus, G' and viscous loss modulus, G'' measured are as shown in Figure 1.26. From the figure it is clear that for small strain amplitudes, the system is elastic and at $\gamma_o \sim 0.03$ it began to loose rigidity. For large strain amplitudes, G' and G'' are nearly the same which is typical behaviour of soft glassy materials[49][16]. Hence the rheological yield strain for this system is $0.020 \leq \gamma_y^{rh} \leq 0.042$ and yield stress is $5.8 \leq \sigma_y^{rh} \leq 11.7$. This yield strain is in accordance with the yield strain obtained from microstructural analysis, Figure 1.25.

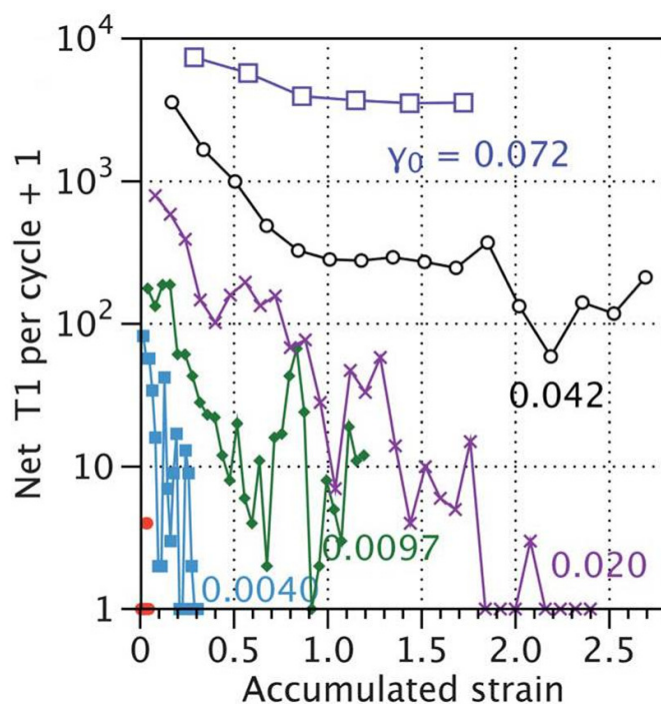


Figure 1.25: Net number of irreversible T1 events plotted as a function of accumulated strain, $\gamma_{acc} - 4N\gamma_o$. Adopted from [48]

It has been observed in colloidal systems, that periodic deformation depends on applied strain amplitude. For small strains, particles are reversible after a short time. But for large strains, a finite fraction of particles are irreversible. Recently, experiments probing the connections between yielding and the onset of irreversibility has been carried out in our laboratory on a binary colloidal glasses[50]. They

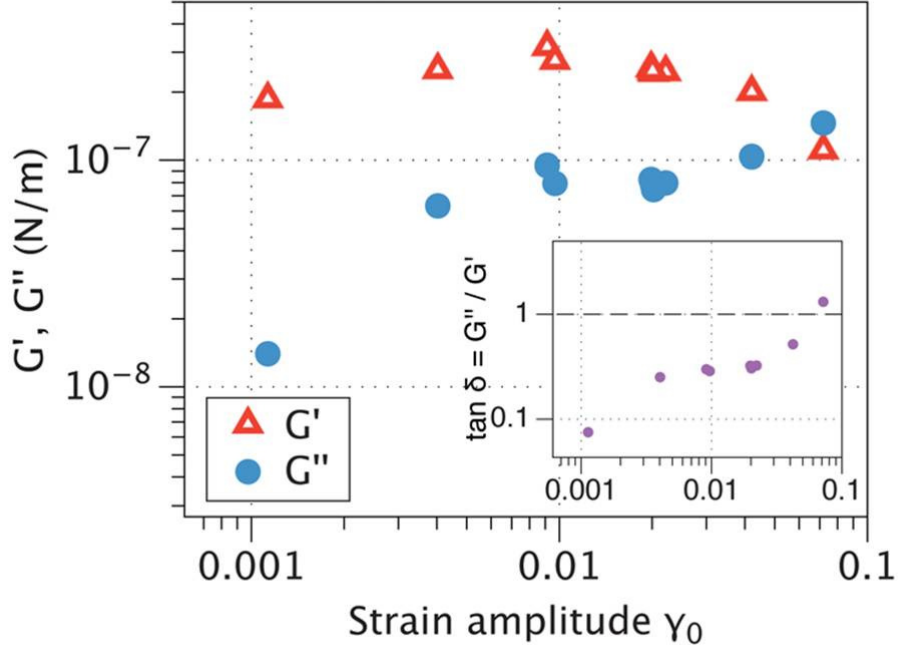


Figure 1.26: Elastic storage modulus, G' and viscous loss modulus, G'' measured as a function of γ_0 . Adopted from [48]

have quantified an absorbing phase transition at the yield point in terms of irreversible particle fraction, f_{IR} measured stroboscopically where f_{IR} serves as order parameter. f_{IR} and viscous loss modulus, G'' are observed to saturate to steady state values similar to [44]. $f_{IR} \sim 0$ for strains below critical strain and $f_{IR} > 0$ above critical strain as shown in Figure 1.23. It is a characteristic of absorbing phase transition [44] and in fact belongs to the conserved direct percolation ($C - DP$) of universality class [51]. Relaxation time as a function of strain in this case fits to the power law, with exponent, $\alpha = 1.1 \pm 0.3$ and order parameter with exponent, $\beta = 0.67 \pm 0.09$. These values are close to exponents of ($C - DP$) universality class [51].

Motivated by the above numerical and experimental studies, we want to understand the yielding of an amorphous system at zero temperature limit, i.e., athermal

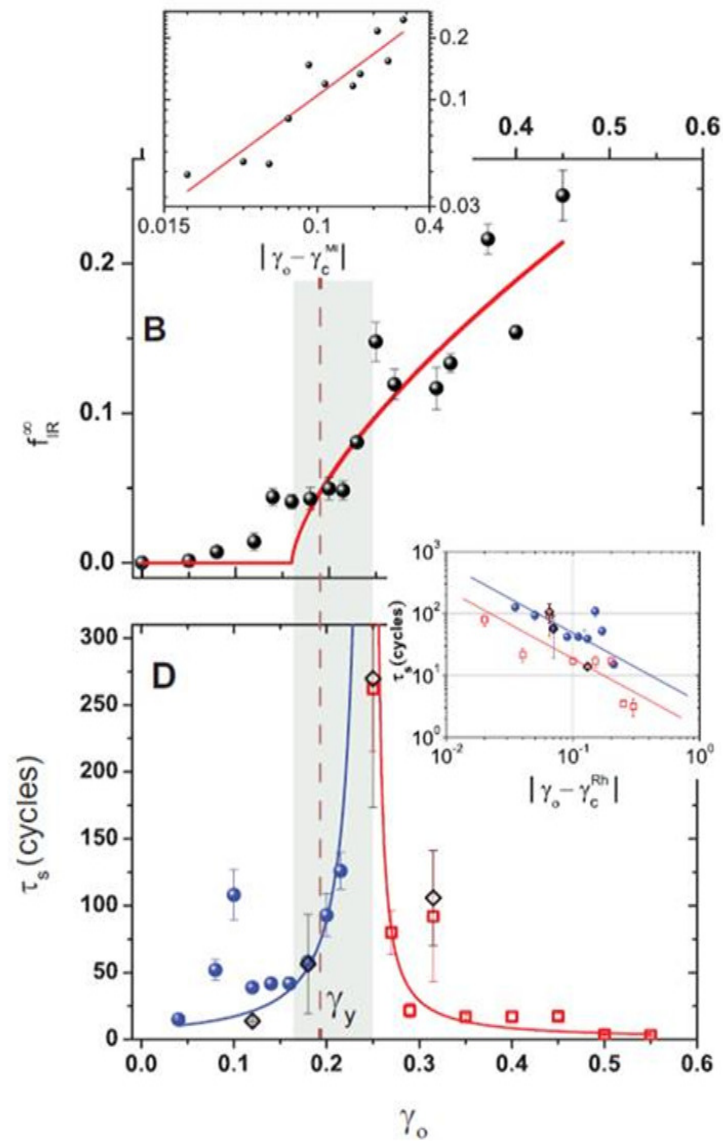


Figure 1.27: f_{IR}^{∞} as a function of γ_o . Inset: $f_{IR}^{\infty} |\gamma_o - \gamma_c^{Mi}|$, Mi corresponds to f_{IR}^{∞} obtained from microscopic analysis. Adopted from [50]

binary amorphous system. Using colloidal systems one cannot access the velocity gradient direction where most of the dynamics can be observed. Hence 2D systems are ideal to probe the dynamics. As an athermal systems we have chosen bubble rafts where there is no thermal motion and friction between the particles. Near yielding, what are the mechanisms that shape the microstructure? Can we

see a phase transition in such systems? Is the dynamics of the system above yield point chaotic? To answer these questions, we have conducted experiments on sheared bubble rafts using rheometry and high speed camera where dynamics can be probed at high spatial and temporal resolution.

CHAPTER 2

EXPERIMENTAL SECTION

As explained in previous chapter, our motivation is to investigate yielding and microstructural dynamics of bubble rafts. In order to shear the bubble raft we have developed a homemade apparatus. This chapter contains description of the set up, interfacial rheometry (interfacial rheometer is used to shear the system of bubble raft) and the procedure to obtain bubble rafts that are stable for long duration.

2.1 Interfacial Rheology

Three dimensional bulk rheology uses continuum mechanics (hydrodynamics) to determine velocity fields, contact forces and the rate of deformation of fluid element in response to an applied shear. In case of interfacial rheology, the continuum is two-dimensional, contact forces are proportional to contact line length and field forces are proportional to unit contact area. When the two fluids that make the interface are simple and pure, interfacial tension has one value and characterises the interface. But the interfaces seen everyday are complex which requires understanding of interfacial viscosity, molecular forces acting in the thin interface layer and surface effects arise due to Marangoni flows. Confining particles, macromolecules, surfactants to an interface induce microstructures with mechanical strength. These microstructures due to hydrodynamic forces gives rise to non-linear rheological

properties that link deformation of interface to the surface stress. Study of complex fluid interfaces give insights into interfacial rheology of foams and emulsions.

An interface can respond to applied surface strain, γ with a corresponding surface stress, and relation between them is given by, $\tau_{ij} = \sigma\delta_{ij} + \frac{\sigma}{\gamma_{ij}}$ where, stress and strain are in tensorial notation. Surface stresses that are present at the interface can induce flow phenomena and flow instabilities. The basis for these phenomena is understood by the equation, $(\tau_{ij}^{(1)} - \tau_{ij}^{(2)}) + \frac{\sigma}{x_i} - \sigma(\nabla \cdot n)n_i = 0$. Superscripts 1 and 2 refer to the separate fluid phases on either side of the interface. This condition shows that the two surface tension contributions balance the stress difference across the interface. The second term in the equation arises due to gradients in surface tension and the third term gives the viscous stress difference. When surface tension acts on interfaces, the resultant stresses are responsible for thinning in liquid films due to capillarity. These capillary forces pump the liquid away from the centre thus subjecting fluid to extensional deformation called the Marangoni effect. For fluid like interfaces with Newtonian behaviour, there is a Boussinesq-Scriven law that relates surface stress to the surface rate of deformation depending on the surface dilation viscosity, μ_d and surface shear viscosity, μ_s . Boussinesq number is defined as the ration of interfacial stresses to bulk stresses given by, $B_o = \frac{\eta_s}{\eta L} = \frac{\text{surfacedrag}}{\text{subphasedrag}}$. For elastic interfaces, surface dilation elastic modulus is defined as, $E = A(\frac{\gamma}{A})$, where A is the surface area. It describes the resistance of interface against surface tension gradient. Surface dilation viscosity affects the rate at which these surface gradients vanish. If the surface is dilated with a frequency f , its response is described by a complex surface dilation modulus, $E^*(f) = E'(f) + iE''(f)$ At high frequency, interface behaves as an insoluble monolayer, $E' \rightarrow E_\infty$ the limiting elasticity and $E'' = 2f_d$. In the zero frequency limit, surfactant exchanges between the bulk and surface and interface does not resist dilation. At intermediate fre-

quency, the interface is viscoelastic. For viscoelastic interfaces, B_o [52] is given by,

$$B_o = \frac{G_s''(\omega) - iG_s'(\omega)}{\omega L \eta} = \frac{\eta_s''(\omega) - i\eta_s'(\omega)}{L \eta}$$

2.1.1 Shear measurements at constant area

Interfacial shear rheology is conducted at constant surface area. In these measurements, interfacial flows are generated either by moving solid boundaries within the interface or by applying gradient in surface pressure. Interfacial rheometers can measure stress and deformation history for fluid interfaces. They also measure fundamental material functions such as shear rate dependent viscosity, linear viscoelastic moduli. Gradients in surface tension should be avoided because they will induce Marangoni effects. Also, B_o should be large enough to trust the measured material properties. This number can be increased by minimizing the characteristic length scale of geometry, L . Interfacial rheometry is used for fatty acids and alcohols, phospholipids, proteins and colloidal particles (spherical and elliptical). Monolayer of colloidal particles at interface exhibit viscoelastic properties.

Based on above discussed factors, results have been obtained. Figure 2.1 shows interface rheological measurements of polystyrene colloidal monolayer at interface of aqueous solution of 0.1M sodium chloride and decane. This monolayer behaves like a viscoelastic interface[53]. The interface is elastic at low frequencies and viscous at high frequencies.

2.1.2 Interfacial Rheometer

Measurement of interfacial properties is challenging due to complexity of flow between interface and bulk. In such cases, B_o becomes a guiding parameter to construct interfacial rheometer. In the B_o as described above, L is length scale of the

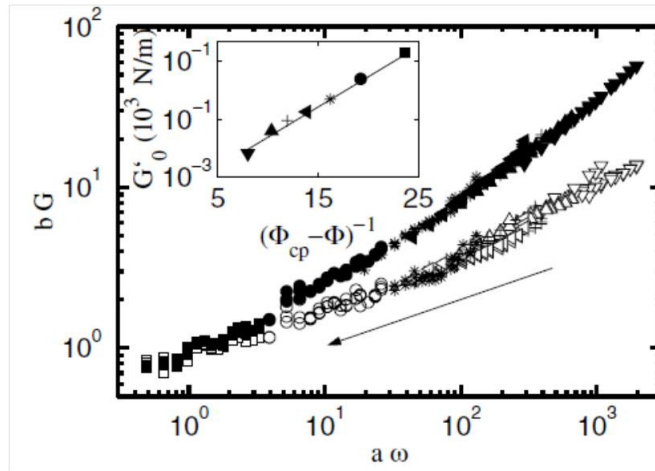


Figure 2.1: Master curve showing log plots of the scaled values of (open symbols) G' and (solid symbols) G'' against the scaled frequency for the monolayer of colloidal particles. The arrow indicates the direction of increasing surface concentration, which coincides with increasing magnitude of moduli. The inset shows an exponential divergence of the elastic modulus as the concentration approaches the close-packing fraction. Adapted from [53]

measuring probe related to ratio of area of measuring probe to the perimeter in contact with the interface. When B_o is larger than 1, drag experienced by the probe at interface dominates and when B_o is smaller than 1, mechanical responses from surrounding sub phases are measured. Hence, main goal of the surface/interface rheometry is to provide greater extent of sensitivity to measure interface properties alone. Thus for an interfacial rheometer very small value of L is recommended.

Based on above mentioned criteria, various viscometers were developed. Mayers and Harkins first reported the development of a 2D capillary viscometer which is guided by surface pressure-driven flow in a channel. Rotational devices offer more flexibility and induce several 2D equivalents of (i) Couette geometry, which is a bicone rheometer or (ii) double wall couette geometry, which is double-wall ring geometry rheometer. Another type is interfacial rod rheometer which is equivalent

to sliding plate rheometer in 3D.

2.2 Experimental Setup

For our experiments we have used MCR 301 Anton Paar rheometer, Germany with a bicone measuring system geometry. Experimental setup is as shown in Figure 2.2. The setup consists of liquid solution in a cylindrical container to generate amorphous raft. A biconal disc is integrated with low friction motor of the rheometer. Figure 2.3 shows the schematic experimental setup. The disc is placed at the surface of liquid which is also an interface between liquid and air. Capillary bore of 0.3 mm attached to an aquarium air pump is used to diffuse air into liquid in a controlled fashion to produce bidispersed rafts by varying depth below the liquid surface. Thus formed raft is stabilised by maintaining humidity (covering the raft). Shear stress either oscillatory or steady is applied on to the raft through the measuring system. The microstructure dynamics is captured using a Photron fast camera SA4 (3600 frames per second; at 1024 X 1024 pixels), attached with a Nikon 60 mm/f2.8D AF Macro lens. A light emitting diode board illuminates the raft uniformly from below. The camera views the raft through a front coated mirror placed 45° to the raft. Both, rheometer and fast camera are connected to work stations and data is collected. The camera can image at very high frame rates and microstructural dynamics is captured at high spatial and temporal resolution.

2.2.1 Stability of the raft

For a long experiment, highly stable raft is required. It is achieved in the manner as described below. To prepare this solution, we have taken equal volumes of glycerol, toy bubble solution (available from super market) and 0.017M Sodium Stearate.

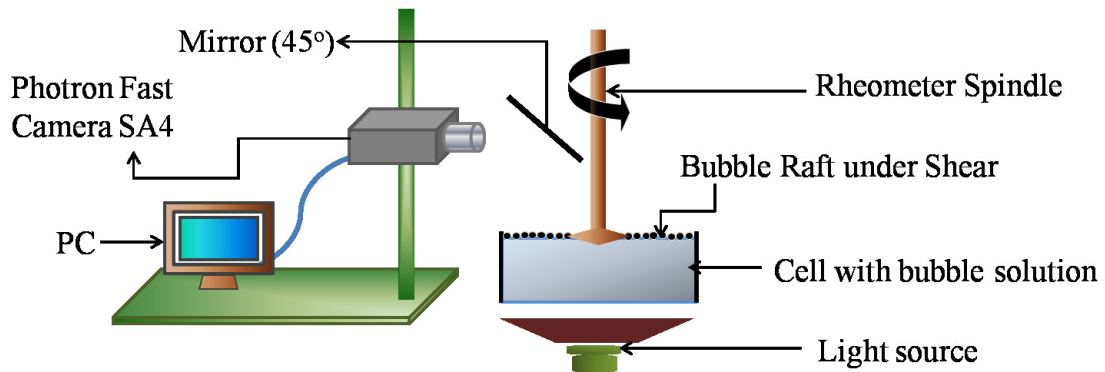


Figure 2.2: Schematic of Experimental setup showing all the instruments and apparatus used

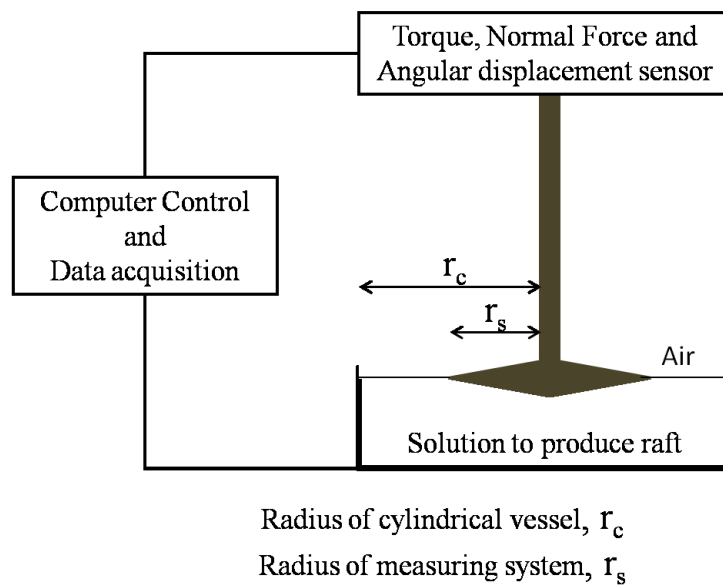


Figure 2.3: Schematic of a biconal disc coupling with a commercial bulk rheometer.

It is observed that the solution ages with time and produce stable rafts. In our experiment, we have observed that the raft is stable for 8-10 hours.

2.2.2 Steps describing how we arrived at the setup

Step-1: We have taken a glass cylindrical cell and roughened the periphery using 3 mm glass beads so that the raft pins to the boundary (ensures no slip).

Step-2: The cell is placed on the rheometer stage plate and rheometer spindle is brought in place. We have designed the geometry of the spindle as bicone with grooves at the rim so that raft gets pinned to it and hence no wall slip at the inner boundary as well.

Step-3: Bubble solution is then transferred into it gently and bubbles of two sizes were blown which makes a binary amorphous system.

Step-4: Thus formed raft at the interface of solution and air is stabilised by covering the raft that can maintain humidity.

Step-5: The raft is then illuminated with a series of LED diodes connected in parallel and spread on a board and placed under the cylindrical cell to give uniform illumination.

Step-6: A front coated mirror is then placed above the raft at an angle of 45°

Step-7: Photron fast camera is then focused and a time series images of the raft are captured.

Step-8: Oscillatory shear strain is applied to the system through the measuring system (spindle) and mechanical response from the raft and microscopic rearrangements of the raft are simultaneously captured. (Oscillatory rheology is explained in the next section)

Step-9: Time series images obtained from video microscopy are analysed using Image J and Matlab. (Image processing is explained in the next section)

2.3 Oscillatory Rheology

Mechanical deformation of many soft systems is complex due to the fact that they are viscoelastic. In such cases, oscillatory rheology can quantify both elastic-like and viscous-like properties of these soft solids at different time scales. Hence it is

an important tool to understand microstructural and dynamic properties of these systems. Rheometer consist of a measuring system with different geometries and can be rotated with a desired angular frequency through which an oscillatory strain is imposed onto the system.

The basic principle of oscillatory rheology is to impose a sinusoidal shear deformation(strain) and measure the resultant stress response from the system. Time scale at which system is probed is determined from frequency of oscillation, ω of the imposed shear strain. Imposed strain is given by, $\gamma(t) = \gamma \sin(\omega t)$ and measure stress response is given by, $\sigma(t)$ which is complex in nature for viscoelastic materials. Applied strain, measured stress for a elastic solid, a viscous liquid and viscoelastic fluid is as shown in Figure 2.4. For purely elastic /Hookean solid, stress is proportional to strain and proportionality constant is shear modulus. Stress is always in-phase with applied strain. For purely viscous/Newtonian liquid, stress is proportional to rate of strain and proportionality constant is viscosity of the fluid. Stress is out-of-phase with applied strain by a phase angle, $\frac{\pi}{2}$ where ω is the frequency of applied strain. Viscoelastic materials show a stress response that is both in-phase and out-of-phase with the applied strain. As a result stress response shows a phase shift with strain which lies between 0 and $\frac{\pi}{2}$. Hence viscoelastic behaviour of the system at a given ω is characterised by the storage modulus, $G'(\omega)$ (solid-like behaviour) and loss modulus, $G''(\omega)$ (liquid like behaviour). Thus, for a sinusoidal shear deformation(strain) $\gamma(t) = \gamma \sin(\omega t)$, stress response for a viscoelastic material is given by $\sigma(t) = G'(\omega)\gamma \sin(\omega t) + G''(\omega)\gamma \cos(\omega t)$.

For a typical oscillatory rheology experiment, $G'(\omega)$ and $G''(\omega)$ are measured at a fixed r or as a function of r at fixed ω . Nonlinear viscoelastic measurements provide valuable information about wide range of soft materials called soft glassy

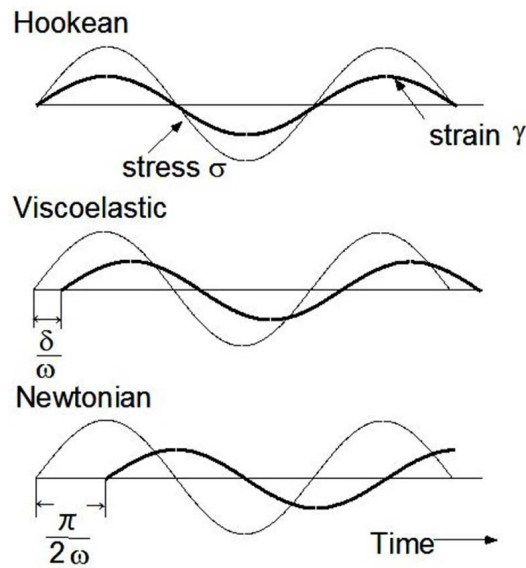


Figure 2.4: Schematic stress response to oscillatory strain deformation for Hookean/elastic solid, Newtonian/viscous liquid, viscoelastic material.

materials[16]. Underlining physics of glassy systems suggests that microstructural relaxation is linked with nonlinear viscoelastic response[54]. At low frequencies, $G'(\omega)$ is dominated and with increase in ω , $G''(\omega)$ initially increases to a peak and decreases at large strains. Hence oscillatory rheology is a beneficial tool to measure complex properties of soft glasses.

2.4 Image processing

Photron fast camera SA4 (maximum frame rate = 3600 frames per second) is used to capture images of the raft at 30 frames per second. Figure 2.6 shows the image of the bubble raft with centres tracked using ImageJ software. Distribution of sizes of the particles is plotted as shown in Figure 2.7. The raft consists of particles of 2 sizes with small particle to big particle number ratio of 2.4.

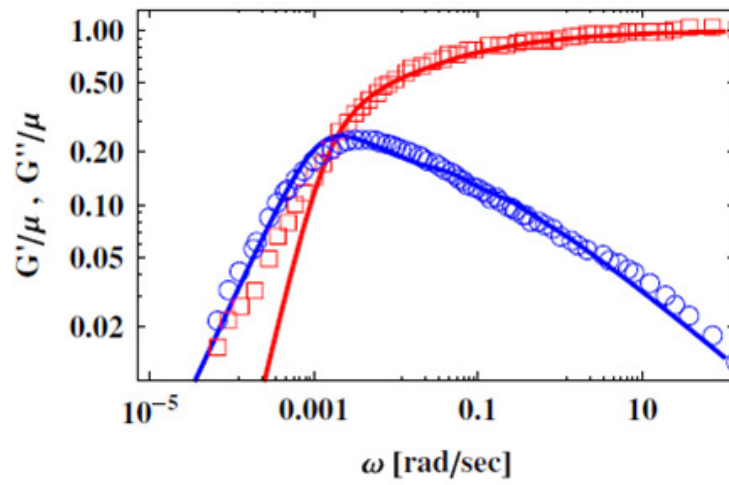


Figure 2.5: Oscillatory measurements of G' (solid circles) and G'' (open circles) for a typical soft glass. Adopted from [55]

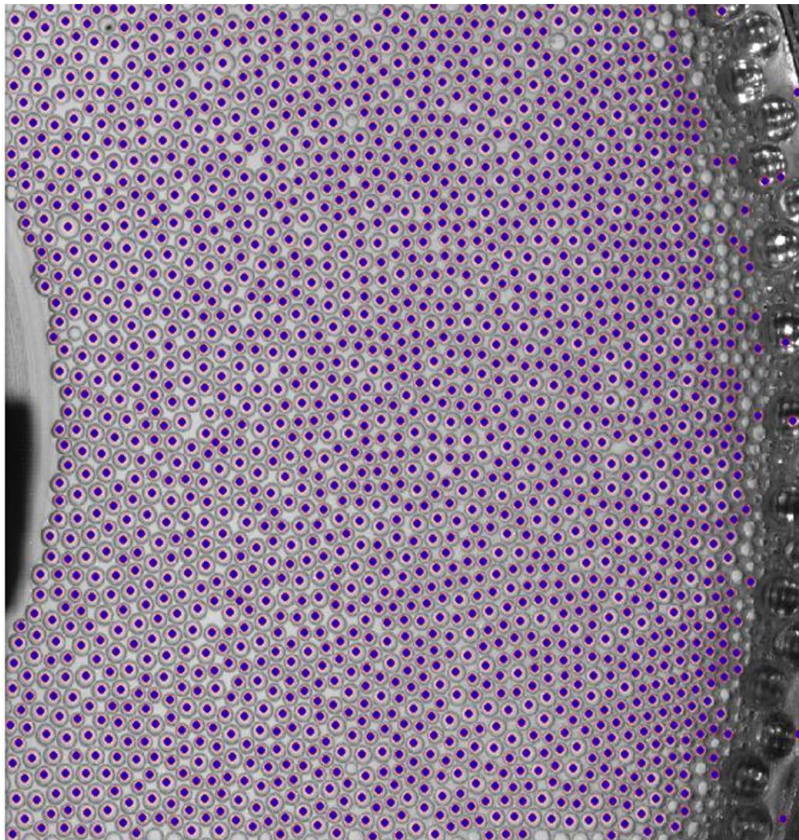


Figure 2.6: Image captured by video microscopy and tracked using ImageJ software.

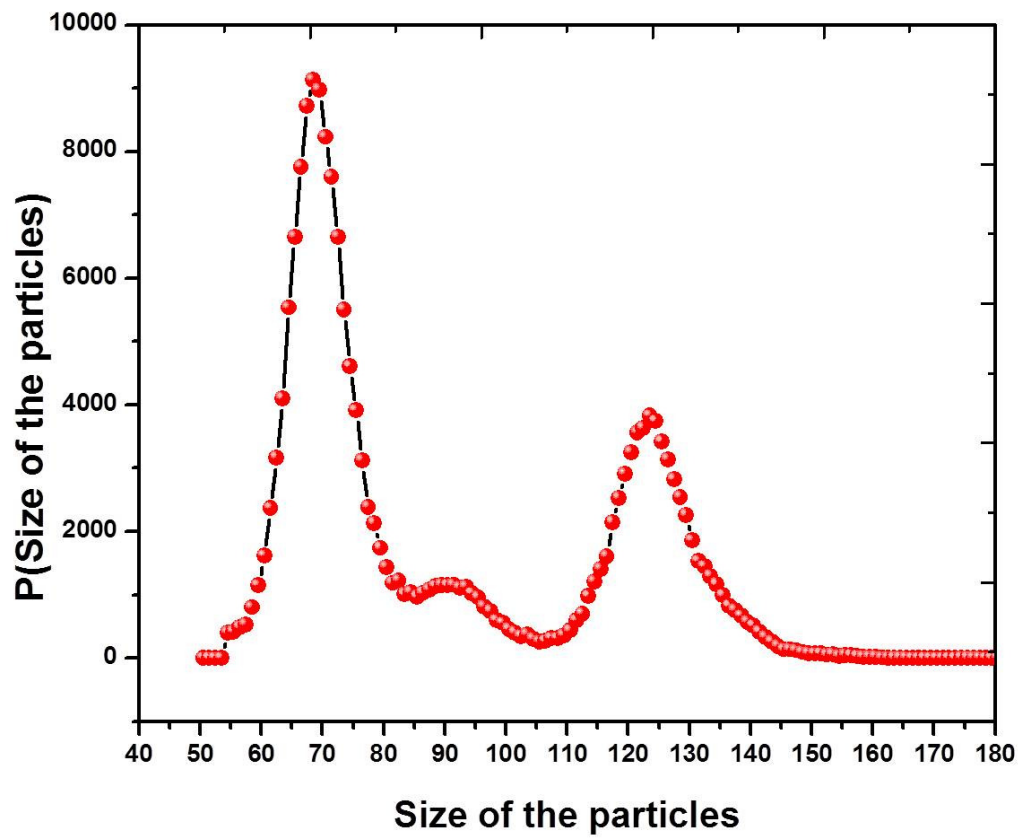


Figure 2.7: Distribution of sizes of particles of the raft obtained from processing images obtained from video microscopy.

CHAPTER 3

YIELDING AND ONSET OF IRREVERSIBILITY IN ATHERMAL AMORPHOUS RAFTS

Although there is growing experimental and theoretical evidence that yielding of soft solids has the hallmarks of a phase transition, experiments thus have suffered from various limitations. These are, (1) Brownian motion is very likely to smear out a sharp transition in colloidal systems. (2) the relevant plane for probing dynamics is the velocity (V), velocity gradient (∇V) plane which is very difficult to access in colloid experiments due to imaging limitations and the dynamics is often probed in the velocity (V), velocity vorticity ($\nabla x V$) plane.

In our experiments, we have used bubble rafts which are two dimensional systems where dynamics is observed in $V, \nabla x V$ plane unlike colloidal systems. Using bubble rafts we wish to understand yielding in athermal amorphous systems and connect it to the onset of irreversible microstructural changes.

3.1 Measurement of yield strain

We have measured the yield strain by performing a linear viscoelastic rheology experiment at a fixed ω of 0.5 rad/s and sweeping across the strain amplitude, γ_o . The elastic storage modulus, G' and the viscous loss modulus, G'' for bubble solution alone and for solution with raft as a function of strain amplitude, γ_o is plotted in Figure 3.1 (a) and Figure 3.1 (b) respectively. The linear viscoelastic

response of the raft was obtained by subtracting the contribution of solution from the measurements of solution with raft. This plot shows a crossover of G' and G'' as shown in Figure 3.2. For small γ_o behaviour of the raft is predominantly elastic (solid like) which is characterised by higher value of storage modulus, G' in comparison to loss modulus, G'' . For high γ_o , raft is predominantly viscous (liquid like). Therefore, γ_o that separates elastic and viscous response of the raft is identified as an yield strain, γ_y . According to generic behaviour for soft glassy materials[16], sheared amorphous systems initially deform elastically due to stored elastic energy up to yield point. Similar behaviour is observed in our system (G' greater than G''). G'' for soft glasses increases (less than G') till yield point and then decreases while being higher than G' . This shows a maximum dissipation energy at the yield point. In contrast to this we have observed G'' to decrease continuously across yield point. In an earlier experiment Keim and Arratia have measured the viscous behaviour of colloidal particles at the oil-water interface. However, they have been unable to measure rheological response beyond the crossover owing to the experimental limitations. In our apparatus we have used a conventional rheometer coupled to a homemade cell through which we have been able to access the response beyond the yield strain. Subsequently, experiments were done at a fixed ω and the dynamics of the system was studied as a function of the number of imposed oscillation cycles for various γ_o across γ_c .

3.2 Microstructural changes accompanying yielding

As described in Chapter 1, amorphous rafts yield through shear induced topological rearrangements, T1 and T2 events. In order to understand the crossover of G' and G'' at $\gamma_c = 0.11$ we have processed and analysed the data captured

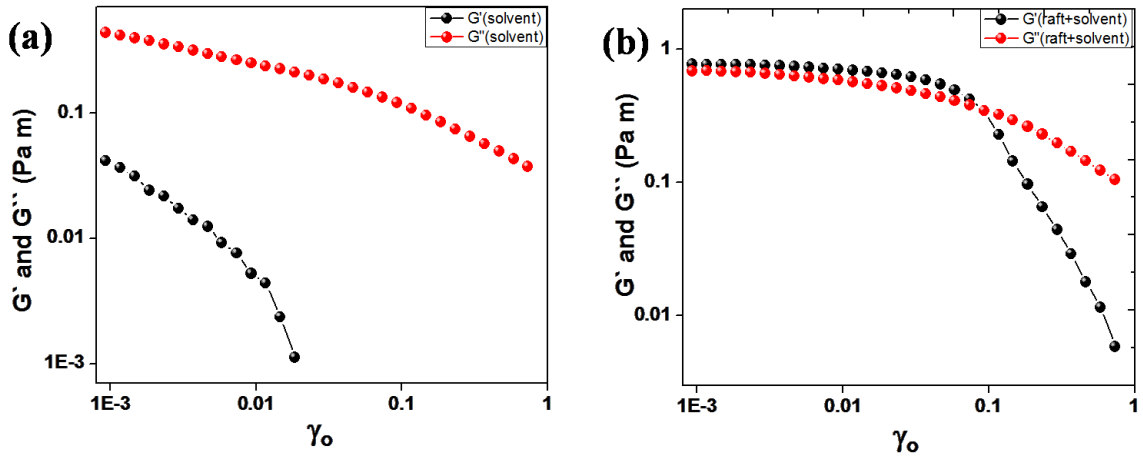


Figure 3.1: Elastic storage modulus, G' (black) and viscous loss modulus, G'' (red) plotted as a function of applied strain, γ for (a) solution/solvent and (b) solvent along with raft.

from the fast camera. Since our experimental system facilitates tracking of individual particles we have identified non-affine events (irreversible T1 events) that leads to plasticity. During every run in the experiment we have not observed any T2 events (refer to section-1.4) and the system is stable. In order to get a microscopic understanding of yielding in amorphous systems, we have studied temporal evolution of irreversible T1 events that leads to the onset of irreversibility.

3.2.1 Algorithm to obtain T1 events

Time series images/frames obtained from the fast camera are preprocessed and particle dynamics is tracked in time following the Matlab codes. Voronoi cell for every particle is constructed and vertices (V), edges (E) and cell numbers (C) are obtained in every frame. Using these V , E , C nearest neighbours (N) and next nearest neighbours (NN) for every cell are identified as shown in Figure 3.3. All N pairs and NN pairs are mapped in time. In order to obtain irreversible

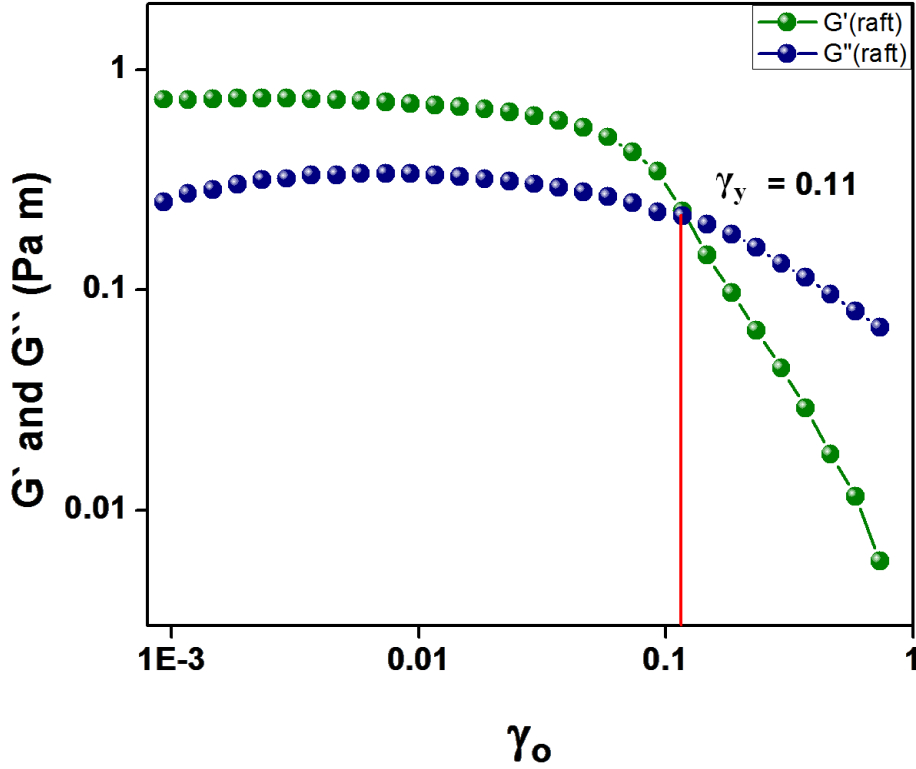


Figure 3.2: Elastic storage modulus, G' and viscous loss modulus, G'' plotted as a function of applied strain, γ for raft (olive green and navy blue - filled circles). γ_y is approximately 0.116.

T1 events, frames are considered stroboscopically (end of each cycle). List of N pairs and NN pairs are now compared and if N^{th} pair in frame at the beginning of the cycle is the NN^{th} pair at the end of cycle, it is picked as a T1 event. Hence, NN pair in frame one is N pair in frame two and vice versa. A pair of N and NN constitute one T1 event. When an oscillatory shear strain is applied in one cycle, four particles participating in a T1 event change their configuration and the changed configuration continues after end of the cycle which explains change in microstructure. To calculate reversible T1 events, frames at the end of every half cycle are considered. This is because reversible events in the positive cycle of

applied shear, change their configuration and comes back to original configuration in negative half cycle. As a result no T1 event is captured. Algorithm described here is shown as a flow chart in Figure 3.4.

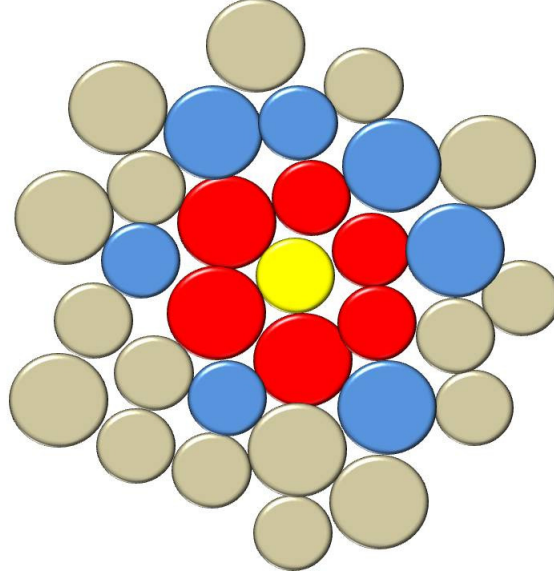


Figure 3.3: Finding nearest neighbours: Red particles are nearest neighbours (N) and blue are next nearest neighbours (NN) for particle marked yellow.

Figures 3.5,3.6,3.7 shows the temporal evolution of # T1 events for γ_o , 0.02,0.10,0.32 respectively for cycle, $t = 1,6,24$. Particles marked red are nearest neighbours and marked blue are next nearest neighbours. A pair of nearest neighbours and a pair of next nearest neighbours constitute a T1 event. For $\gamma_o = 0.02$ # T1 events goes to zero where as for $\gamma_o \geq 0.10$ # T1 events shows a finite value even at long times (cycle number).

3.2.2 Irreversible T1 events

The total # irreversible T1 events for every cycle ($f_{T1}(t)$) obtained from above described algorithm is plotted as a function of cycle number(t) as shown in Figure 3.8. # irreversible T1 events are initially very large and decays to zero for small

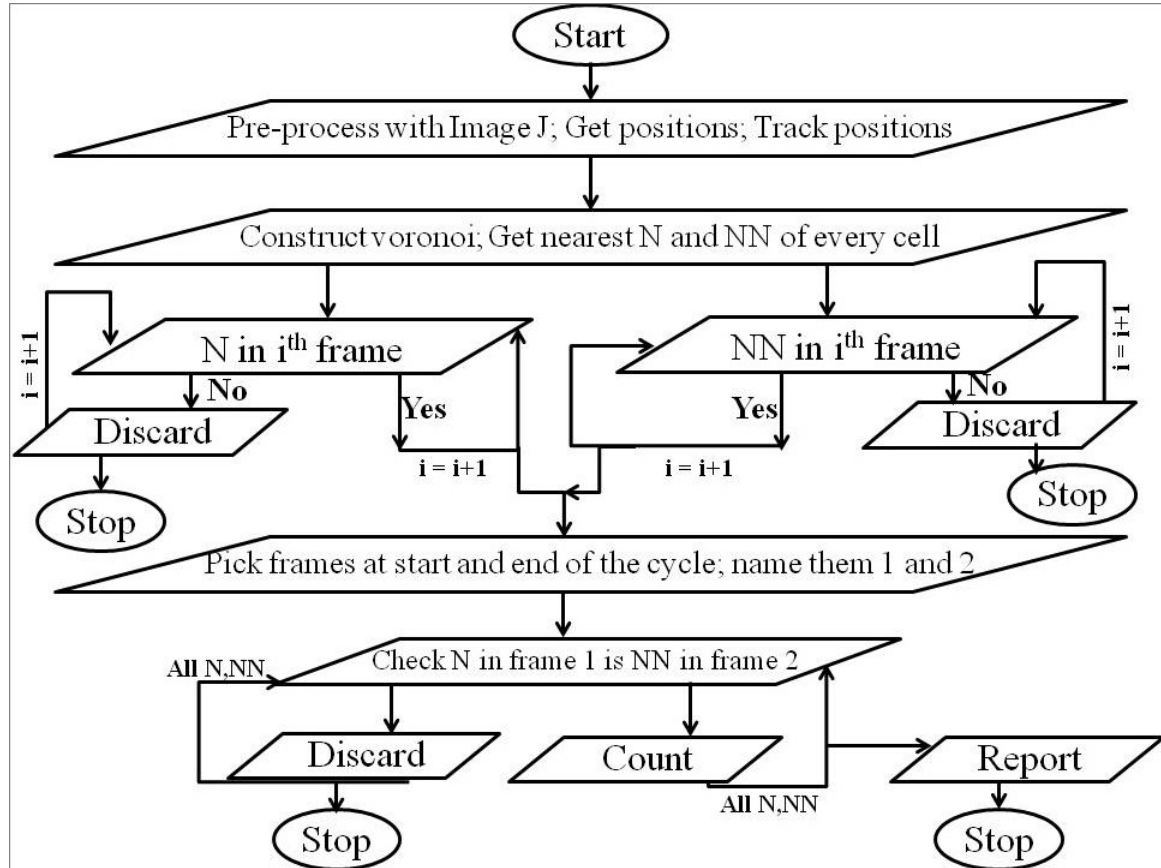


Figure 3.4: Flow chart explaining the algorithm to find T1 events.

strain amplitudes, suggesting that the system has attained a steady state. For large strain amplitudes, number of irreversible T1 events decays to a finite value is the characteristic of fluctuating steady state. The initial value of $\#$ T1 events is denoted by f_{T1}^0 and steady state value by f_{T1}^∞ . To probe the connection between yielding and microscopic irreversibility, we now focus on the temporal evolution of irreversible T1 events as a function of γ_o at fixed ω .

3.2.3 Steady state Irreversible T1 events as order parameter

We have characterised γ_o dependence of $\#$ irreversible T1 events at steady state denoted by f_{T1}^∞ and is plotted as a function of γ_o as shown in Figure 3.9.

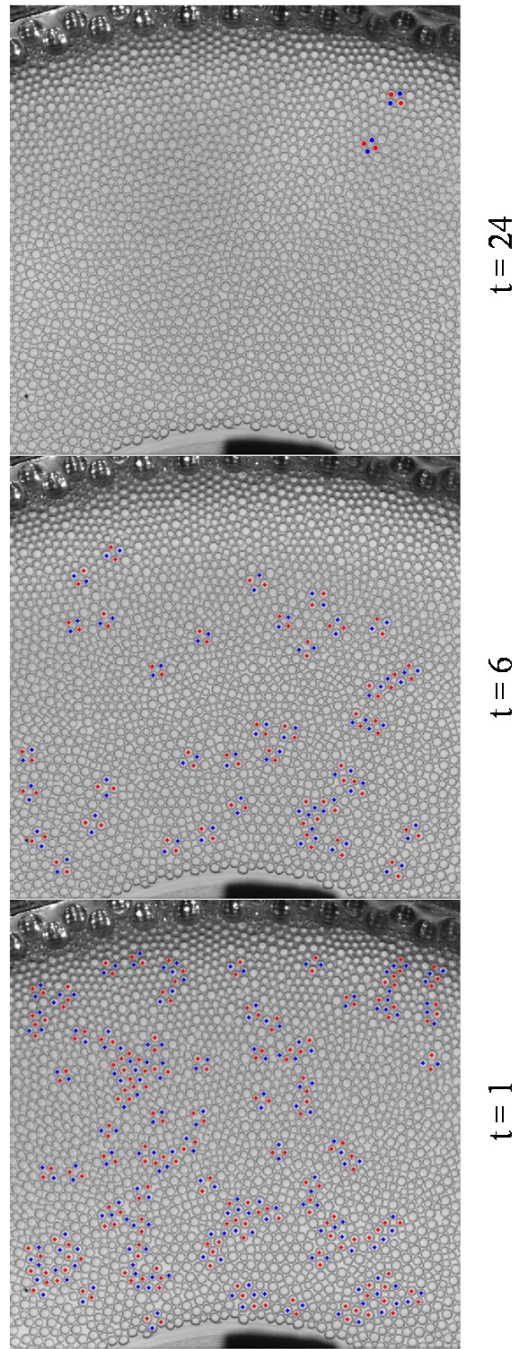


Figure 3.5: Temporal evolution of $\#$ T1 events for $\gamma_o = 0.02$. Cycle numbers for corresponding figure is given below the figure.

f_{T1}^∞ is almost zero for small γ_c and shows a sudden increase beyond certain γ_o and saturates to a higher value at very large γ_c . This shows that there is a sharp onset

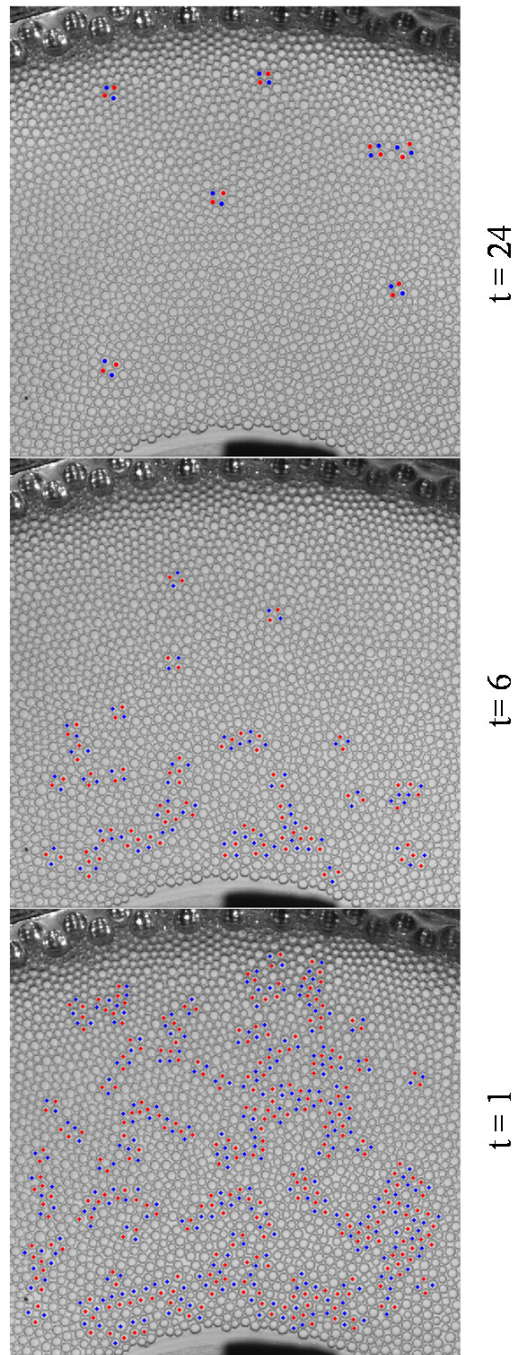


Figure 3.6: Temporal evolution of $\#$ T1 events for $\gamma_o = 0.10$. Cycle numbers for corresponding figure is given below the figure.

of irreversibility beyond certain γ_o and we consider this γ_o as a critical strain γ_c . Above the critical strain, γ_c , f_{T1}^∞ plotted as a function of $(\gamma - \gamma_c)$ on log-log scale is

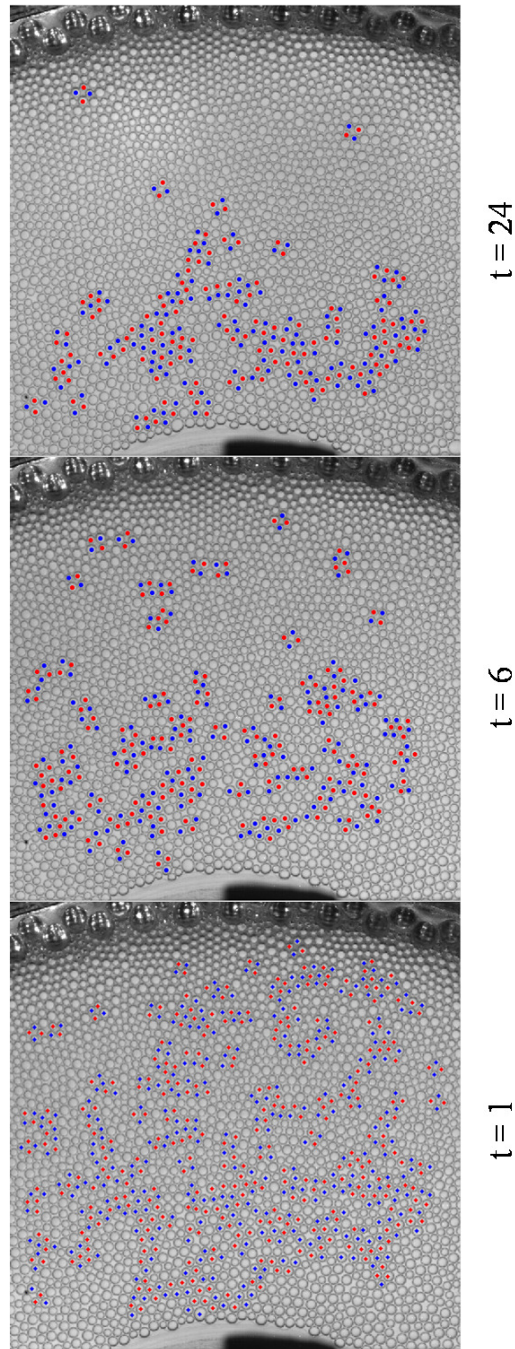


Figure 3.7: Temporal evolution of $\#$ T1 events for $\gamma_o = 0.32$. Cycle numbers for corresponding figure is given below the figure.

shown in Figure 3.9(Inset). f_{T1}^∞ data is best fitted to the power law, $f_{T1}^\infty = (\gamma - \gamma_c)^\beta$ for $\gamma_c = 0.1$ which coincides with γ_y , where the exponent $\beta = 0.34 \pm 0.05$. Although

the value of exponent obtained does not coincide with colloid experiment, the behaviour of f_{T1}^∞ versus γ_o is reminiscent of an absorbing phase transition and hence f_{T1}^∞ serves as an order parameter for this transition.

Time at which f_{T1} saturates to a steady state shows a critical divergence in

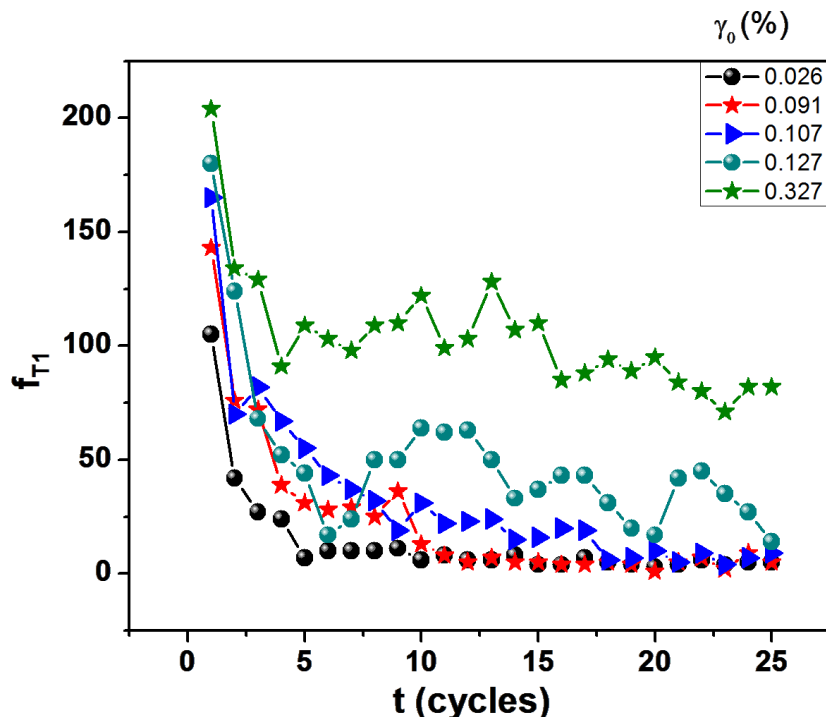


Figure 3.8: Number of irreversible T1 events plotted as a function of cycle number. Individual strain is marked by the colour code shown.

the vicinity of γ_c . In order to extract relaxation time τ , $f_{T1}(t)$ for all strains is smoothened to remove noise. It is then fitted to the functional form, $f_{T1}(t) = (f_{T1}^0 - f_{T1}^\infty) \frac{e^{-t/\tau}}{t^\delta} + f_{T1}^\infty$ which captures the transition from exponential to powerlaw behaviour in the vicinity of the critical point [41][44]. τ is the relaxation time (in terms of cycles) for $f_{T1}(t)$ to reach a steady state, t is the cycle number and δ is the power law exponent which is almost constant for all the strains. The time scale, τ plotted as a function of γ_o as shown in Figure 3.10 is suggestive of divergence

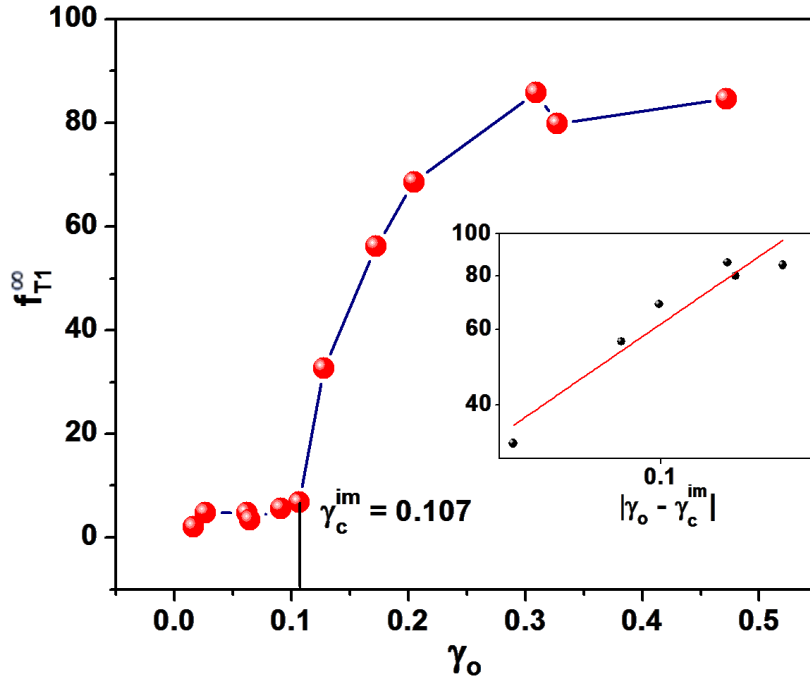


Figure 3.9: Number of irreversible T1 events at steady state, f_{T1}^{∞} is plotted against applied strains (corrected strains). Inset: f_{T1}^{∞} above critical strain, γ_c is plotted as a function of $(\gamma - \gamma_c)$. Exponent obtained is $\beta = 0.34 \pm 0.05$.

at critical strain. Within the experimental certainty, γ_c from the fits was found to be remarkably close to the γ_y obtained from rheology measurements. Figure 3.10 inset shows τ plotted as a function of $|\gamma_o - \gamma_c|$ (log-log plot) fits to the power law, $\tau = (|\gamma_o - \gamma_c|)^{\nu}$, where the exponent is obtained to be $\nu = 0.83 \pm 0.18$ for data below γ_c .

3.3 Interface fluctuations

In experiments, granular/amorphous systems are observed to show shear banding. Since T1 events in our experiment are found to evolve in time, we want to

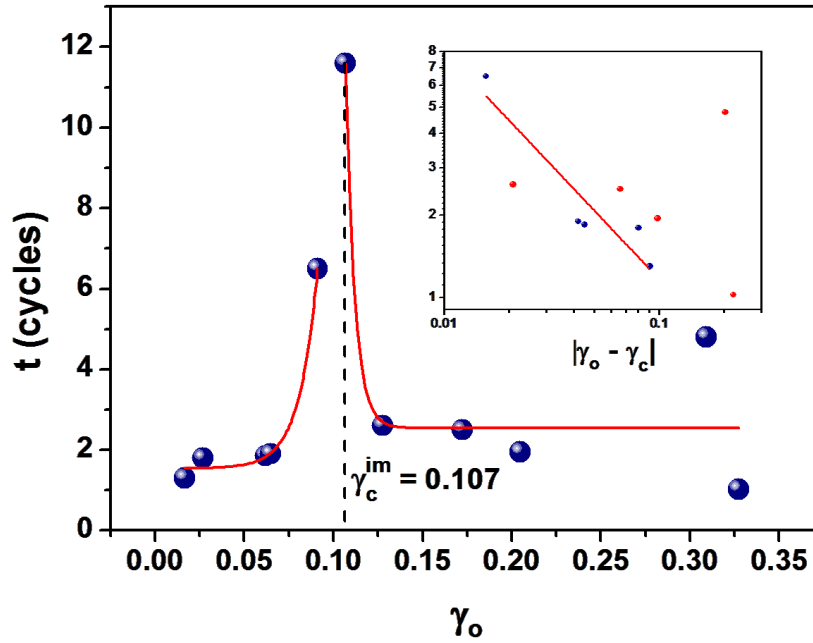


Figure 3.10: Relaxation time, τ as a function of applied strain (γ_o). Solid curve is the power law fit to the data. Inset: Exponent obtained for power law fit $\tau = (|\gamma_o - \gamma_c|)^\nu$ is $\nu = 0.83 \pm 0.18$. Blue for data below γ_c and red for data above γ_c

investigate their consequences on the evolution of shear bands. To connect the evolution of number of irreversible T1 events to the shear banding, we have looked at the fluctuations of the shear band interface. Owing to the radial symmetry of the system, we have divided the system into sections/bands whose width is roughly one particle diameter. velocity profile of the raft is plotted as a function of radius, r as shown in Figure 3.11. While for small strains, $\gamma_o < 0.1$, $V(r)$ only shows small deviation from linearity, for $\gamma_o > 0.1$ In order to understand the dynamics of shear band interface, we have plotted velocity profile for first ten oscillatory strain cycles for the interface which is seven particle diameters from the spindle. The velocity profile was then divided into two linear regions and the intersection their intersection is identified as the shear band which is six to seven particle diameters (σ) from

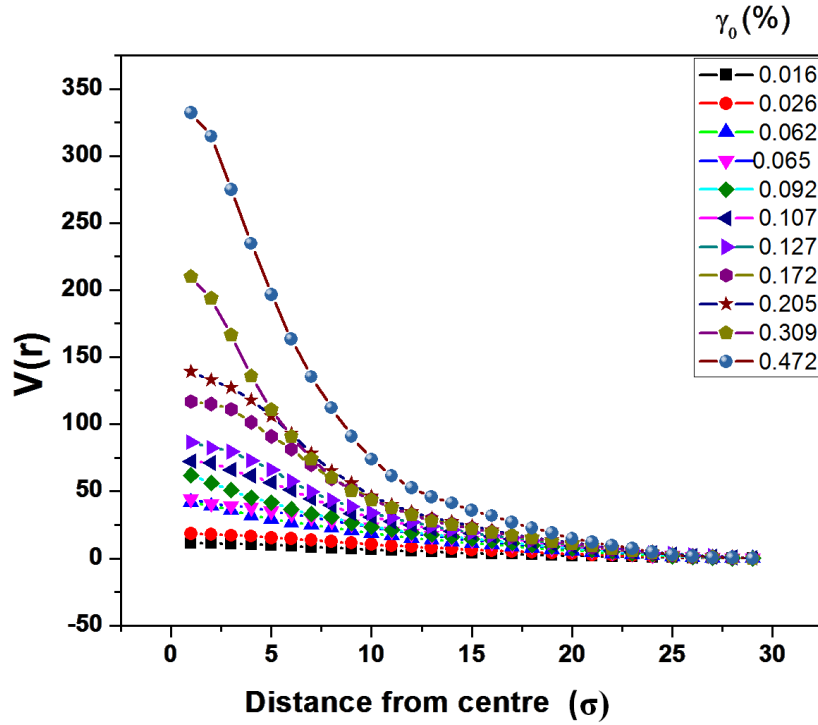


Figure 3.11: Velocity $V(\theta)$ as a function of distance from the spindle.

the spindle as shown in Figure 3.12. Further velocity profile was found to evolve in time. For $\gamma_o < 0.1$ while the $V(r)$ reaches a steady state in about fifteen cycles, for $\gamma_o > 0.1$ $V(r)$ shows larger fluctuations which is consistent with T1 events saturating at a finite value giving rise to irreversibility. It is observed to evolve in time as shown in Figure 3.13.

In order to quantify the spatial fluctuations of the shear band interface as a function of γ_o , we have calculated $d'(x, t) = d(x, t) - \langle d(x) \rangle_t$. $d'(x, t)$, distribution of interface fluctuations is plotted as shown in Figure 3.14 and observed that width of these distributions increase with γ_o . Figure 3.15 shows width of the distribution as a function of γ_o . From the figure it is clear that there is a change in slope for the curve near the critical strain γ_c . The γ_c obtained from Figure 3.15, coincides

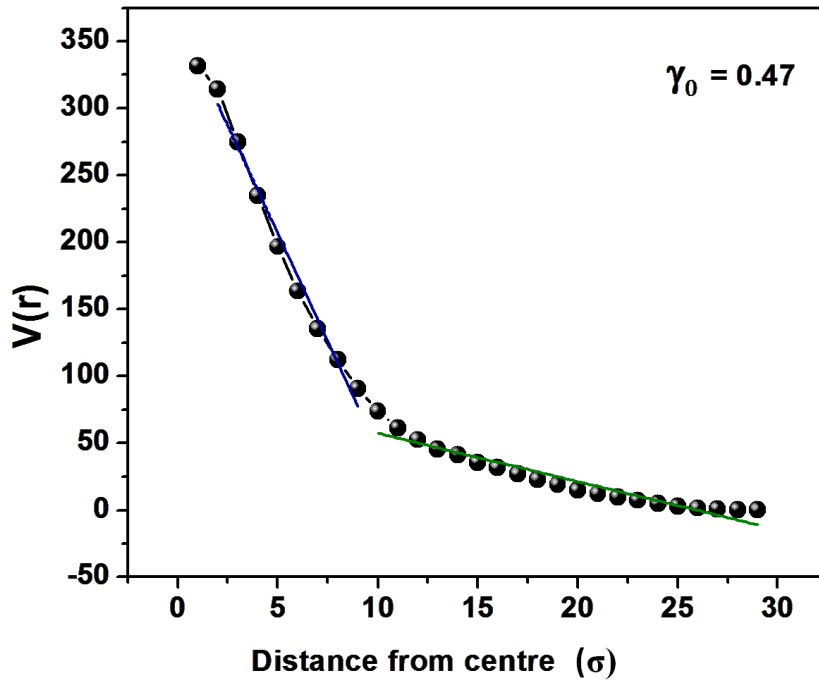


Figure 3.12: Velocity $V(\theta)$ for $\gamma_o = 0.47$ as a function of distance from the spindle showing change in slope at the interface.

with the yield strain γ_y obtained from rheology measurements. This behaviour is typically seen in the roughening transition of interfaces[56] and it is tempting to wonder if a similar behaviour is occurring in the vicinity of γ_c .

3.4 Steady state measurements of G' and G''

Elastic storage modulus, G' and viscous loss modulus, G'' are measured as a function of number of cycles (τ) and plotted as shown in Figure 3.16 and Figure 3.17. G' for all strains increases and then saturates to a finite value after certain number of cycles (it shows a trend). G'' shows an increase below critical strain and

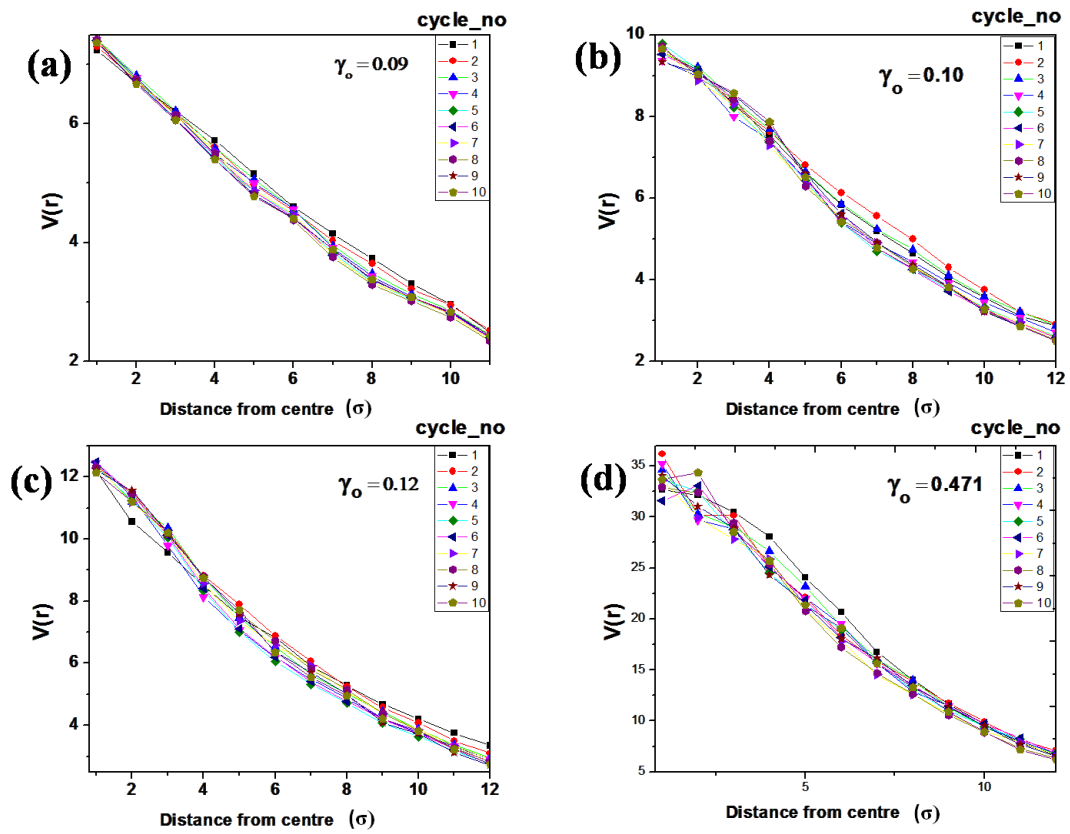


Figure 3.13: Velocity $V(\theta)$ as a function of distance from the spindle for first 10 cycles.

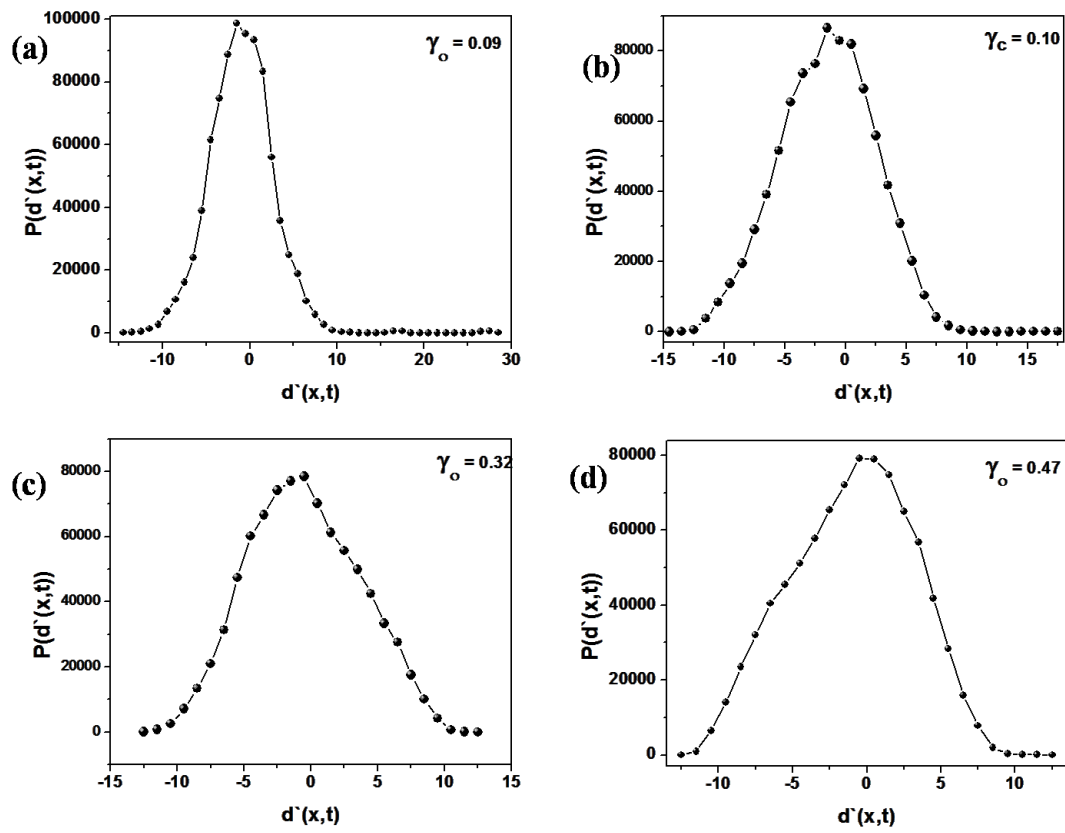


Figure 3.14: Distribution of interface fluctuations $d'(x, t)$.

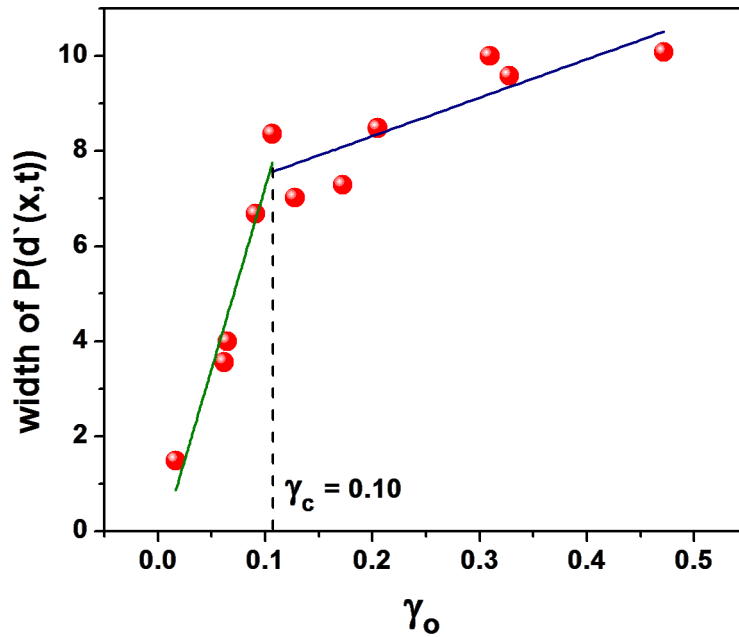


Figure 3.15: Width of distribution of interface fluctuations as a function of γ_o .

increase then decrease above critical strain. Efforts are underway to understand these results.

3.5 Conclusion

The experimental setup is efficient for studying microstructural dynamics of athermal system for longer duration experiments. Having commercial rheometer coupled with bubble raft cell, we were able to measure mechanical response of the raft beyond yield point unlike in other experiments. Connections between yielding and microstructural behaviour of the raft has been studied. The relaxation time τ is suggestive of a divergence at γ_c and f_{T1}^∞ serves as an order parameter and is indicative of an absorbing phase transition near γ_y . Our results complement

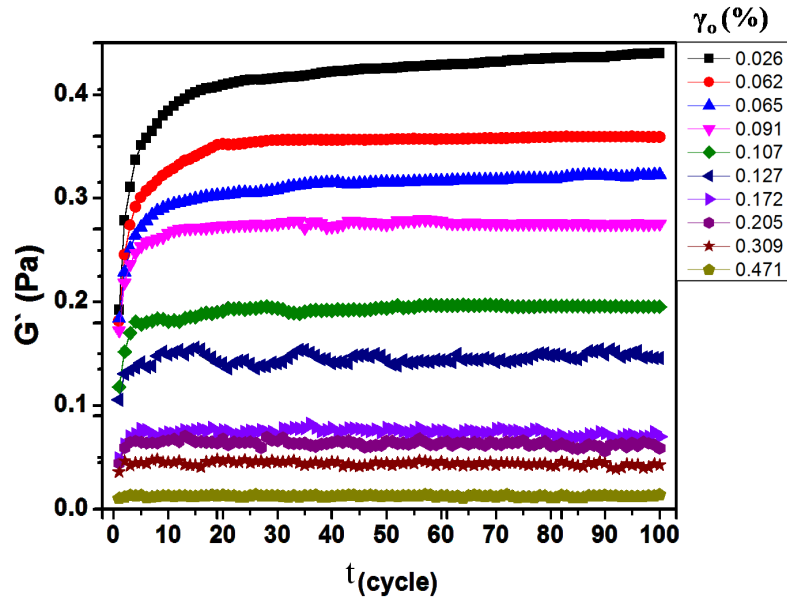


Figure 3.16: Elastic storage modulus, G' as a function of cycle number, τ . Individual strain is marked by the colour code shown.

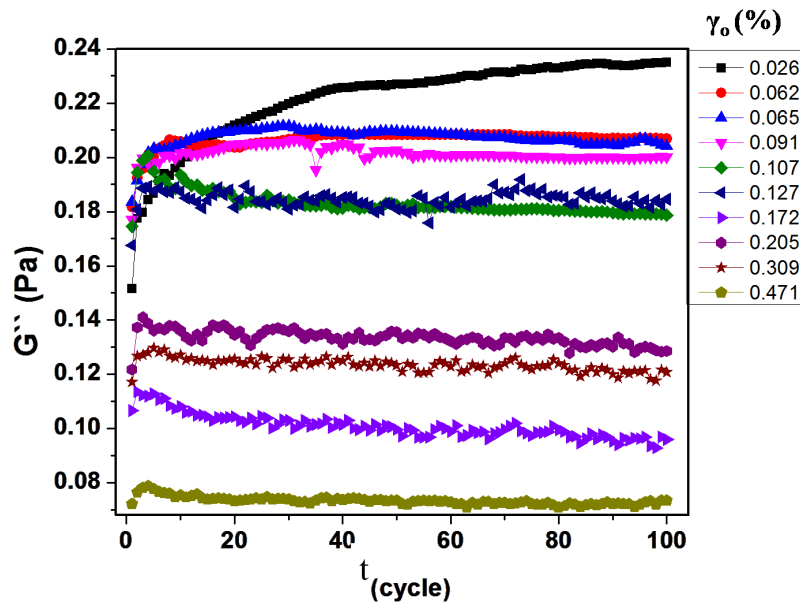


Figure 3.17: Elastic storage modulus, G'' as a function of cycle number, τ . Individual strain is marked by the colour code shown.

experiments on colloidal systems where an absorbing phase transition near yielding was recently observed. It is tempting to speculate that the behaviour observed in our system is generic to other soft solids such as gels, emulsions etc.

3.6 Future of our experiments

Similar to granular systems that can undergo transition from chaotic (characterised by Lyapunov exponent) to jammed state[57], there is a possibility that bubble rafts can exhibit a transition to chaotic state. This is evident from Figure 3.5, T1 event number above critical strain (yield point) is finite in the fluctuating steady state. So our future experiments are aimed to understand the chaotic nature of the system and characterize it using Lyapunov exponent. Because we have access to look at deformation/strain field and can measure forces on individual particles, we want to connect irreversible T1 events that occur in group/clusters and force chains. Moreover our results suggest that there is a roughening transition at γ_o which is in agreement with yielding. Hence we planned to investigate and understand this smooth to roughening transition at the yield/critical strain, γ_c/γ_c and quantify roughness of the interface.

References

- [1] C. A. Angell, *Formation of Glasses from Liquids and Biopolymers*, *Science* **267**, 1924 (1995).
- [2] L. Berthier and G. Biroli, *Theoretical perspective on the glass transition and amorphous materials*, *Rev. Mod. Phys.* **83**, 587 (2011).
- [3] I. N. Levine, *Physical Chemistry* (Tata McGraw-Hill, , 2007).
- [4] P. G. Debenedetti and F. H. Stillinger, *Supercooled liquids and the glass transition*, *Nature* **410**, 259 (2001).
- [5] Callister, *Principles of Physical Metallurgy* (Tata McGraw-Hill, , 2007).
- [6] C. Maloney and A. Lemaitre, *Universal Breakdown of Elasticity at the Onset of Material Failure*, *Phys. Rev. Lett.* **93**, 195501 (2004).
- [7] A. van Blaaderen and P. Wiltzius, *Real-Space Structure of Colloidal Hard-Sphere Glasses*, *Science* **270**, 1177 (1995).
- [8] R. G. Larson, *The structure and Rheology of Complex Fluids* (Oxford University Press, , 1999).
- [9] P. Schall, D. A. Weitz, and F. Spaepen, *Structural Rearrangements That Govern Flow in Colloidal Glasses*, *Science* **318**, 1895 (2007).

-
- [10] W. van Meegen, T. C. Mortensen, S. R. Williams, and J. Müller, *Measurement of the self-intermediate scattering function of suspensions of hard spherical particles near the glass transition*, Phys. Rev. E **58**, 6073 (1998).
- [11] K. N. Pham *et al.*, *Yielding of colloidal glasses*, EPL (Europhysics Letters) **75**, 624 (2006).
- [12] A. Argon, *Plastic deformation in metallic glasses*, Acta Metallurgica **27**, 47 (1979).
- [13] A. Argon and H. Kuo, *Plastic flow in a disordered bubble raft (an analog of a metallic glass)*, Materials Science and Engineering **39**, 101 (1979).
- [14] L. Bragg and J. F. Nye, *A Dynamical Model of a Crystal Structure*, Proceedings of the Royal Society of London. Series A. Mathematical and Physical Sciences **190**, 474 (1947).
- [15] L. Bragg and W. M. Lomer, *A Dynamical Model of a Crystal Structure. II*, Proceedings of the Royal Society of London. Series A. Mathematical and Physical Sciences **196**, 171 (1949).
- [16] P. Sollich, F. m. c. Lequeux, P. Hébraud, and M. E. Cates, *Rheology of Soft Glassy Materials*, Phys. Rev. Lett. **78**, 2020 (1997).
- [17] E. Pratt and M. Dennin, *Nonlinear stress and fluctuation dynamics of sheared disordered wet foam*, Phys. Rev. E **67**, 051402 (2003).
- [18] F. Da Cruz, F. Chevoir, D. Bonn, and P. Coussot, *Viscosity bifurcation in granular materials, foams, and emulsions*, Phys. Rev. E **66**, 051305 (2002).
- [19] C. W. Macosko, *Rheology : Principles, measurements, and applications* (Wiley-VCH,USA, , 2002).

-
- [20] D. J. DURIAN, D. A. WEITZ, and D. J. PINE, *Multiple Light-Scattering Probes of Foam Structure and Dynamics*, *Science* **252**, 686 (1991).
- [21] R. Höhler, S. Cohen-Addad, and H. Hoballah, *Periodic Nonlinear Bubble Motion in Aqueous Foam under Oscillating Shear Strain*, *Phys. Rev. Lett.* **79**, 1154 (1997).
- [22] A. Gopal and D. Durian, *Shear-Induced “Melting” of an Aqueous Foam*, *Journal of Colloid and Interface Science* **213**, 169 (1999).
- [23] M. Dennin and C. M. Knobler, *Experimental Studies of Bubble Dynamics in a Slowly Driven Monolayer Foam*, *Phys. Rev. Lett.* **78**, 2485 (1997).
- [24] A. Abd el Kader and J. C. Earnshaw, *Shear-Induced Changes in Two-Dimensional Foam*, *Phys. Rev. Lett.* **82**, 2610 (1999).
- [25] G. Debrégeas, H. Tabuteau, and J.-M. di Meglio, *Deformation and Flow of a Two-Dimensional Foam under Continuous Shear*, *Phys. Rev. Lett.* **87**, 178305 (2001).
- [26] J. Lauridsen, M. Twardos, and M. Dennin, *Shear-Induced Stress Relaxation in a Two-Dimensional Wet Foam*, *Phys. Rev. Lett.* **89**, 098303 (2002).
- [27] B. Dollet *et al.*, *Two-dimensional flow of foam around an obstacle: Force measurements*, *Phys. Rev. E* **71**, 031403 (2005).
- [28] I. Cantat and R. Delannay, *Dissipative flows of 2D foams*, *The European Physical Journal E* **18**, 55 (2005).
- [29] T. Herdtle and H. Aref, *Numerical experiments on two-dimensional foam*, *Journal of Fluid Mechanics* **241**, 233 (1992).

-
- [30] D. A. Reinelt and A. M. Kraynik, *Simple shearing flow of a dry Kelvin soap foam*, Journal of Fluid Mechanics **311**, 327 (1996).
- [31] S. Vincent-Bonnieu, R. Höhler, and S. Cohen-Addad, *Slow viscoelastic relaxation and aging in aqueous foam*, Europhys. Lett. **74**, 533 (2006).
- [32] A. Kabla and G. Debrégeas, *Local Stress Relaxation and Shear Banding in a Dry Foam under Shear*, Phys. Rev. Lett. **90**, 258303 (2003).
- [33] D. M. Wang Y, Krishan K, *Impact of boundaries on velocity profiles in bubble rafts*, Phys. Rev. E. **73**, (2006).
- [34] C. E. Maloney and A. Lemaitre, *Amorphous systems in athermal, quasistatic shear*, Phys. Rev. E **74**, 016118 (2006).
- [35] G. Katgert, B. P. Tighe, and M. van Hecke, *The jamming perspective on wet foams*, Soft Matter **9**, 9739 (2013).
- [36] A. KABLA and G. DEBREGAS, *Quasi-static rheology of foams. Part 1. Oscillating strain*, Journal of Fluid Mechanics **587**, 23 (2007).
- [37] A. KABLA, J. SCHEIBERT, and G. DEBREGAS, *Quasi-static rheology of foams. Part 2. Continuous shear flow*, Journal of Fluid Mechanics **587**, 45 (2007).
- [38] P. Bak, C. Tang, and K. Wiesenfeld, *Self-organized criticality*, Phys. Rev. A **38**, 364 (1988).
- [39] T. Okuzono and K. Kawasaki, *Intermittent flow behavior of random foams: A computer experiment on foam rheology*, Phys. Rev. E **51**, 1246 (1995).

- [40] G. DRAZER, J. KOPLIK, B. KHUSID, and A. ACRIVOS, *Deterministic and stochastic behaviour of non-Brownian spheres in sheared suspensions*, Journal of Fluid Mechanics **460**, 307 (2002).
- [41] I. M. Jánosi, T. Tél, D. E. Wolf, and J. A. C. Gallas, *Chaotic particle dynamics in viscous flows: The three-particle Stokeslet problem*, Phys. Rev. E **56**, 2858 (1997).
- [42] D. J. Pine, J. P. Gollub, J. F. Brady, and A. M. Leshansky, *Chaos and threshold for irreversibility in sheared suspensions*, Nature **438**, 997 (2005).
- [43] G. Taylor, *Dispersion of Soluble Matter in Solvent Flowing Slowly through a Tube*, Proceedings of the Royal Society of London. Series A. Mathematical and Physical Sciences **219**, 186 (1953).
- [44] L. Corte, P. M. Chaikin, and D. J. Pine, *Random organization in periodically driven systems*, Nat Phys **4**, 420 (2008).
- [45] R. Dickman *et al.*, *Critical behavior of a one-dimensional fixed-energy stochastic sandpile*, Phys. Rev. E **64**, 056104 (2001).
- [46] I. Regev, T. Lookman, and C. Reichhardt, *Onset of irreversibility and chaos in amorphous solids under periodic shear*, Phys. Rev. E **88**, 062401 (2013).
- [47] D. Fiocco, G. Foffi, and S. Sastry, *Oscillatory athermal quasistatic deformation of a model glass*, Phys. Rev. E **88**, 020301 (2013).
- [48] N. C. Keim and P. E. Arratia, *Yielding and microstructure in a 2D jammed material under shear deformation*, Soft Matter **9**, 6222 (2013).
- [49] T. G. Mason *et al.*, *Osmotic pressure and viscoelastic shear moduli of concentrated emulsions*, Phys. Rev. E **56**, 3150 (1997).

- [50] K. H. Nagamanasa, S. Gokhale, A. K. Sood, and R. Ganapathy, *Direct Evidence for an Absorbing Phase Transition Governing Yielding of a Soft Glass*, arxiv **0**, 0 (2014).
- [51] G. I. Menon and S. Ramaswamy, *Universality class of the reversible-irreversible transition in sheared suspensions*, Phys. Rev. E **79**, 061108 (2009).
- [52] T. Verwijlen, P. Moldenaers, H. A. Stone, and J. Vermant, *Study of the Flow Field in the Magnetic Rod Interfacial Stress Rheometer*, Langmuir **27**, 9345 (2011).
- [53] P. Cicuta, E. J. Stancik, and G. G. Fuller, *Shearing or Compressing a Soft Glass in 2D: Time-Concentration Superposition*, Phys. Rev. Lett. **90**, 236101 (2003).
- [54] K. Miyazaki, H. M. Wyss, D. A. Weitz, and D. R. Reichman, *Nonlinear viscoelasticity of metastable complex fluids*, EPL (Europhysics Letters) **75**, 915 (2006).
- [55] E. Bouchbinder and J. S. Langer, *Linear Response Theory for Hard and Soft Glassy Materials*, Phys. Rev. Lett. **106**, 148301 (2011).
- [56] T. O. E. Skinner, D. G. A. L. Aarts, and R. P. A. Dullens, *Grain-Boundary Fluctuations in Two-Dimensional Colloidal Crystals*, Phys. Rev. Lett. **105**, 168301 (2010).
- [57] E. J. Banigan, M. K. Illich, D. J. Stace-Naughton, and D. A. Egolf, *The chaotic dynamics of jamming*, Nature Physics **9**, 288 (2013).